

Biostatistics (2025), **0**, 0, pp. 1–??
doi:10.1093/biostatistics/TSI/biostatistics.arxiv

Unlocking the Power of Time-Since-Infection Models: Data Augmentation for Improved Instantaneous Reproduction Number Estimation

JIASHENG SHI, YIZHAO ZHOU, JING HUANG*

Department of Biostatistics, Epidemiology, and Informatics, Perelman School of Medicine,

University of Pennsylvania, Philadelphia, USA

jing14@pennmedicine.upenn.edu

SUMMARY

The Time Since Infection (TSI) models, which use disease surveillance data to model infectious diseases, have become increasingly popular due to their flexibility and capacity to address complex disease control questions. However, a notable limitation of TSI models is their primary reliance on incidence data. Even when hospitalization data are available, existing TSI models have not been crafted to improve the estimation of disease transmission or to estimate hospitalization-related parameters - metrics crucial for understanding a pandemic and planning hospital resources. Moreover, their dependence on reported infection data makes them vulnerable to variations in data quality. In this study, we advance TSI models by integrating hospitalization data, marking a significant step forward in modeling with TSI models. We introduce hospitalization propensity parameters to jointly model incidence and hospitalization data. We use a composite likelihood function to accommodate complex data structure and an Monte Carlo expectation–maximization algorithm to estimate model parameters. We analyze COVID-19 data to estimate disease transmission, assess risk factor impacts, and calculate hospitalization propensity. Our model improves the accuracy of estimating the instantaneous reproduction number in TSI models, particularly

*To whom correspondence should be addressed.

when hospitalization data is of higher quality than incidence data. It enables the estimation of key infectious disease parameters without relying on contact tracing data and provides a foundation for integrating TSI models with other infectious disease models.

Key words: Composite likelihood function; Hospitalization propensity; Infectious disease transmission; Time between diagnosis and hospitalization.

1. INTRODUCTION

Mathematical modeling is essential for understanding infectious disease transmission, especially during the early stages of pandemics when vaccines, treatments, and immunity are limited. Policy-makers rely on key metrics like the instantaneous reproduction number (R_t), projected incidence, and hospitalization counts to make timely decisions. Various modeling approaches, including compartmental models, agent-based simulations, and time-series analyses, help estimate these metrics. Among these, Time-Since-Infection (TSI) models have gained prominence due to their ability to estimate R_t directly from incidence data using renewal equation concepts.

The concept of TSI models originated in the 1910s by Ross (1916) and Ross and Hudson (1917a,b) and was mathematically formalized by Kermack and McKendrick (1927). They gained further prominence with contributions from Wallinga and Teunis (2004) and Fraser (2007). Recognition in the statistics community grew after the work of Cori *and others* (2013) and the development of the EpiEstim R package (Cori, 2021), which enabled widespread use for real-time R_t estimation, particularly during the COVID-19 pandemic (Pan *and others*, 2020; Gostic *and others*, 2020; Nash *and others*, 2022). Recent enhancements include regression integrations, addressing delays, and multi-location analyses (Quick *and others*, 2021; Shi *and others*, 2022; Ge *and others*, 2023). These models are based on the idea that new infections depend on three factors: recent infection counts, the current reproduction number, and how transmission evolves over time. They are mathematically linked to renewal equations, which model new cases as a sum of

past infections weighted by infectious potential, and have similarities with branching processes that describe how each case leads to secondary infections (Athreya *and others*, 2004; Lloyd-Smith *and others*, 2005). Tools like the EpiNow2 package (Abbott *and others*, 2021) have applied these concepts to estimate time-varying transmission dynamics, accommodating various infectiousness patterns and reporting delays.

Compared to other infectious disease models, e.g., compartmental models, TSI models are valued for their practicality and flexibility. Their statistical foundation enables integration with advanced methods, making them well-suited for complex modeling challenges. By relying primarily on empirical data, TSI models require minimal epidemiological knowledge, making them particularly useful during new infectious disease outbreaks with limited biological insights (Jewell, 2021). A key advantage is their ability to estimate R_t directly from incidence data alone, making them user-friendly during early pandemic stages when other surveillance data are scarce. However, this reliance on incidence data can introduce biases from underreporting or reporting delays. Moreover, when other crucial data, such as hospitalization counts, become available, traditional TSI models are not equipped to integrate this information. It is because they assume each new infection is linked to prior cases, a pattern not followed by hospitalization data. This limitation restricts TSI models from effectively modeling disease-related hospitalizations, an essential metric for assessing pandemic trajectory and planning healthcare resources.

This study aims to address these limitations by developing an enhanced TSI model that integrates hospitalization data. We investigate whether incorporating hospitalization data can improve the precision of R_t estimates and offer insights into disease dynamics and severity in TSI models. Specifically, our approach aims to: 1) reduce bias in R_t estimation from incidence data inaccuracies, 2) estimate hospitalization-related parameters for assessing disease severity, and 3) combine the strengths of TSI and compartmental models for pandemic response. To achieve this, we introduce a new set of parameters, the hospitalization propensity, which quantifies the ten-

dency of infectious individuals being hospitalized over time since infection. By incorporating hospitalization data into the TSI framework, we use a composite likelihood function to jointly model incidence and hospitalization counts, capturing their interdependent dynamics (Lindsay, 1988; Varin *and others*, 2011). The composite likelihood approach simplifies the modeling of complex data dependencies, allowing us to retain key statistical properties while reducing computational challenges. Using a Monte Carlo expectation–maximization (MCEM) algorithm, which combines stochastic sampling with iterative parameter estimation to handle missing data, we estimate model parameters and assess their accuracy through simulations and an analysis of COVID-19 data across U.S. counties. Our results demonstrate the enhanced precision of R_t estimation and highlight the capability of the proposed framework in supporting hospital resource planning and evaluating local transmission risks.

This work contributes to the field by unlocking the potential of TSI models through data augmentation of incidence and hospitalization data, which refines real-time estimation of R_t , enables the estimation of hospitalization-related parameters previously accessible primarily through contact tracing, and facilitates analysis of associations between risk factors and disease transmission dynamics. The sections that follow outline the methodology, implementation strategy, and broader implications for infectious disease modeling.

2. METHODS

We first provide a brief overview of the fundamentals of TSI models, and then describe the proposed approach to integrate incidence data with hospitalization data based on the TSI framework.

2.1 *Model and Notations*

We use subscripts t to denote calendar time and s to indicate time since infection. Consider a discrete-time setting where I_t represents the number of new infections on day t . Given the infection history up to day $t - 1$, the expected new infections on day t can be expressed as

$E(I_t | I_0, \dots, I_{t-1}) = R_t \Lambda_t$, where $\Lambda_t = \sum_{s=1}^t I_{t-s} \omega_s$ represents the infection potential on day t . This potential is shaped by the current number of infectious individuals and the infectiousness function ω_s , which describes how infectious an individual is s days after infection, with $\sum_{s=0}^{+\infty} \omega_s = 1$. Typically, ω_s is set to zero for $s = 0$ and for $s > \eta$, where η is the time between infection and recovery. This function is often approximated using the distribution of the serial interval or generation time (Svensson, 2007), and estimating R_t involves assuming a distribution for I_t and applying methods like maximum likelihood or Bayesian approaches with predefined values of ω_s (Cori and others, 2013; WHO Ebola Response Team, 2014; Quick and others, 2021).

By “hospitalization”, we refer to hospital admission due to the infectious disease. Let H_t denote the number of new hospitalizations on day t . We define the filtrations $\mathcal{F}_t = \sigma(\{I_r, 0 \leq r \leq t\})$ and $\mathcal{G}_t = \sigma(\{I_r, H_r, 0 \leq r \leq t\})$ which represent the information on past infections and the combined information on both past infections and hospitalizations, respectively. In line with the original TSI models, we assume the number of new infections at time t , given the number of previously infected individuals, follows a Poisson distribution:

$$I_t | \mathcal{F}_{t-1} \sim \text{Poisson}(R_t \Lambda_t), \quad (2.1)$$

Next, we introduce a new set of parameters, the hospitalization propensity of an infected individual, $\tilde{\omega}_s$, which describes the tendency that an infected individual will be hospitalized s days after infection, independent of the calendar time t . For each infected individual, $\tilde{\omega}_s$ represents the probability that hospitalization occurs s days after infection. For the entire infected population, it represents the proportion of individuals hospitalized s days post-infection. Similar to $\{\omega_s\}$, the set $\{\tilde{\omega}_s\}$ satisfies the conditions $\tilde{\omega}_s \geq 0$ and $\sum_s \tilde{\omega}_s = 1$.

We denote $h_{t,s}$ as the number of patients infected at calendar time t and admitted at calendar time $t + s$, i.e., time s since infection, with $\mathbb{E}(h_{t,s} | \mathcal{F}_t) = \tilde{\omega}_s I_t$. If hospitalization does not occur within a certain period $\tilde{\eta}$, we assume $h_{t,s} = 0$ and $\tilde{\omega}_s = 0$ for $s > \tilde{\eta}$ for all t , where the positive integer $\tilde{\eta}$ represents the duration from infection to the time after which the likelihood of

hospitalization becomes negligible. Patients infected at time t and never hospitalized are denoted by $h_{t,-1}$ with the tendency $\tilde{\omega}_{-1} = 1 - \sum_{s=0}^{\tilde{\eta}} \tilde{\omega}_s$. Thus, total incidence I_t and total hospitalizations H_t at time t are connected through

$$I_t = h_{t,-1} + \sum_{s \geq 0} h_{t,s}, \quad \text{and} \quad H_t = \sum_{s=0}^t h_{t-s,s}, \quad \text{for } t = 0, 1, 2, \dots. \quad (2.2)$$

Based on the above setup, we further assume

$$(h_{t,-1}, h_{t,0}, \dots, h_{t,\tilde{\eta}}) \mid I_t \sim \text{Multinomial}(I_t, \tilde{\omega}_{-1}, \tilde{\omega}_0, \dots, \tilde{\omega}_{\tilde{\eta}}). \quad (2.3)$$

From (2.2) and (2.3), we can see the time-series infection and hospitalization data are deeply interconnected and overlapping (1). To model R_t in relation to risk factors, we assume a regression structure inspired by *Shi and others (2022)* and *Quick and others (2021)*:

$$f_{link}(R_t) = X_t^T \beta + \sum_{i=1}^q \theta_i f_i(D_{1,t}, D_{2,t}, D_{3,t}), \quad (2.4)$$

where $t \geq q > 0$ and X_t is a p -dimensional vector that includes a constant 1 and a vector of risk factors of disease transmission, Z_t , such as temperature, social distancing measures, and population density. Here, β represents the effect size of these exogenous variables on transmission. The link function $f_{link}(\cdot)$ transforms R_t , allowing it to be expressed as a linear combination of predictors, e.g., the log link function is one of the most commonly used link functions for non-negative outcomes, while $f_i(\cdot)$ represent a functions of past outcomes. Additionally, we define

$$D_{1,t} = \{X_r\}_{0 \leq r \leq t}, \quad D_{2,t} = \{I_r, \mathbb{E}(H_r)\}_{0 \leq r \leq t-1}, \quad D_{3,t} = \{R_r\}_{0 \leq r \leq t-1}. \quad (2.5)$$

With $D_{1,t}$ being observed, equation (2.4) ensures that $R_t \in \mathcal{F}_t$. Therefore, the second term in (2.4) captures the temporal structure of disease transmission, while the θ_i 's characterize the level of temporal dependency and continuity in the time series of $\{R_t\}_{t \geq 0}$. By combining (2.1)-(2.5), we build a TSI model for hospitalization and incidence data. Indeed, the terms $\{\mathbb{E}(H_r)\}_{1 \leq r \leq t-1}$ in $D_{2,t}$ can be expressed as functions of the hospitalization propensity and the R_t according to

our model. This implies $D_{2,t} \subset \sigma(\{I_r, R_r\}_{0 \leq r \leq t-1})$ and hospitalization data are linked with the disease transmission through the hospitalization propensity. In a broader context, one could substitute $D_{2,t}$ in (2.5) with $\{I_r, H_r\}_{0 \leq r \leq t-1}$. We have reserved this general setting to the Supplementary Materials, focusing here on the model shown in Equation (2.5).

2.2 Composite Likelihood Function

Specifying the full likelihood function for the proposed model is challenging. Specifically, the joint distribution of (I_r, H_r) given \mathcal{G}_{r-1} for $0 \leq r \leq t$ is difficult to retrieve due to the convolution structure outlined in Equation (2.2), the irregular boundaries and range restrictions applied to $\{I_r, H_r\}_{0 \leq r \leq t}$, and the fact that $h_{t,s}$ are often unobserved in practice. Therefore, we adopt a composite likelihood approach to estimate the model parameters. Specifically, we use joint distribution of (I_r, H_r) given \mathcal{F}_{r-1} instead of \mathcal{G}_{r-1} to construct a composite log-likelihood function

$$\ell_C = \sum_{0 \leq r \leq t} \log \mathbb{P}(H_r, I_r \mid \mathcal{F}_{r-1}). \quad (2.6)$$

We derive (2.6) by summing over all possible values of $\{h_{r-s,s}\}_{1 \leq s \leq \tilde{\eta}}$ in the joint distribution of (H_r, I_r) and $\{h_{r-s,s}\}_{1 \leq s \leq \tilde{\eta}}$ conditioning on \mathcal{F}_{r-1} . To achieve this, we first demonstrate in the following lemma that $h_{t,s}$ given \mathcal{F}_{t-1} follows a Poisson distribution and that h_{t,u_1} and h_{t,u_2} are independent given \mathcal{F}_{t-1} when $u_1 \neq u_2$. Then we derive the form of individual component $\mathbb{P}(H_r, I_r \mid \mathcal{F}_{r-1})$ based on this lemma.

Lemma 1 For arbitrary $t > 0$, $-1 \leq u_1, u_2 \leq \min\{t, \tilde{\eta}\}$ and $u_1 \neq u_2$, we have

$$h_{t,u_1} \mid \mathcal{F}_{t-1} \sim \text{Poisson}(\tilde{\omega}_{u_1} R_t \Lambda_t), \quad h_{t,u_2} \mid \mathcal{F}_{t-1} \sim \text{Poisson}(\tilde{\omega}_{u_2} R_t \Lambda_t), \quad (2.7)$$

and $h_{t,u_1} \mid \mathcal{F}_{t-1} \perp h_{t,u_2} \mid \mathcal{F}_{t-1}$. Moreover, $(h_{t,u_1}, h_{t,u_2}) \mid \mathcal{G}_{t-1} = (h_{t,u_1}, h_{t,u_2}) \mid \mathcal{F}_{t-1}$, and $h_{t,u_1} \mid \mathcal{G}_{t-1} \perp h_{t,u_2} \mid \mathcal{G}_{t-1}$.

According to Equation (2.3) and Lemma 1, if we use $\mathbb{1}(\cdot)$ to denote the indicator function, which equals 1 when its condition is true and 0 otherwise, the joint distribution of (H_r, I_r) and

$\{h_{r-s,s}\}_{1 \leq s \leq \tilde{\eta}}$ conditioning on \mathcal{F}_{r-1} can be expressed as the product of the probability density functions of several binomial distributions and two Poisson distributions as follows:

$$\begin{aligned}
 & \mathbb{P}(H_r, I_r, h_{r-\tilde{\eta}, \tilde{\eta}}, \dots, h_{r-1,1} \mid \mathcal{F}_{r-1}) \\
 &= \mathbb{P}\left(h_{r-\tilde{\eta}, \tilde{\eta}}, \dots, h_{r-1,1}, h_{r,0} = H_r - \sum_{s=1}^{\tilde{\eta}} h_{r-s,s}, \sum_{s=-1,1, \dots, \tilde{\eta}} h_{r,s} = I_r - H_r + \sum_{s=1}^{\tilde{\eta}} h_{r-s,s} \mid \mathcal{F}_{r-1}\right) \\
 &= \prod_{s=1}^{\tilde{\eta}} \mathbb{P}\left(\text{Binomial}(I_{r-s}, \tilde{\omega}_s) = h_{r-s,s}\right) \mathbb{1}\left(H_r - I_r \leq \sum_{s=1}^{\tilde{\eta}} h_{r-s,s} \leq H_r\right) \\
 &\quad \cdot \mathbb{P}\left(\text{Poisson}(\tilde{\omega}_0 R_r \Lambda_r) = H_r - \sum_{s=1}^{\tilde{\eta}} h_{r-s,s}\right) \\
 &\quad \cdot \mathbb{P}\left(\text{Poisson}((1 - \tilde{\omega}_0) R_r \Lambda_r) = I_r - H_r + \sum_{s=1}^{\tilde{\eta}} h_{r-s,s}\right)
 \end{aligned} \tag{2.8}$$

Therefore, the joint distribution of (H_r, I_r) conditioning on \mathcal{F}_{r-1} can be calculated by summing over all possible values of $\{h_{r-s,s}\}_{1 \leq s \leq \tilde{\eta}}$,

$$\mathbb{P}(H_r, I_r \mid \mathcal{F}_{r-1}) = \sum_{h_{r-\tilde{\eta}, \tilde{\eta}}, \dots, h_{r-1,1}} \mathbb{P}(H_r, I_r, h_{r-\tilde{\eta}, \tilde{\eta}}, \dots, h_{r-1,1} \mid \mathcal{F}_{r-1}). \tag{2.9}$$

3. INFERENCE

3.1 Estimation

In this section, we describe the procedures for estimating model parameters using MCEM algorithms, where the missing data $\{h_{r-s,s}\}_{1 \leq s \leq \tilde{\eta}}$ are unobserved tracing information and the observed disease data consist of daily incidence and hospitalization counts. Let $\gamma = (\beta, \theta, \omega, \tilde{\omega}) \in \Gamma$ denote the model parameters, where β and θ define a time series model for the instantaneous reproduction number $\{R_t\}_{t \geq 1}$, as described in equation (2.4). The terms $\{R_t\}_{t \geq 1}$ are integrated into the composite likelihood function (2.6) through (2.8) and (2.9), introducing β and θ as parameters to be estimated. We use notations like \mathbb{P}_γ to indicate that the probability is associated with the parameter value γ . We use γ_0 to denote the parameter values corresponding to the underlying true data-generating mechanism, and $\hat{\gamma}$ denote the maximum composite likelihood

estimator. The composite likelihood function integrates information from both the observed data and the modeled structure of $\{R_t\}_{t \geq 1}$, and the EM algorithm addresses the missing data, enabling the joint estimation of all parameters γ . To improve the efficiency of sampling the missing data $h_{r-\tilde{\eta}}, \dots, h_{r-1,1}$ in the algorithm, we incorporate an acceptance-rejection sampling method.

Let $Data_{obs,r} = \{X_j, I_j\}_{0 \leq j \leq r} \cup \{H_r\}$ denote the observed data and $Data_{miss,r} = \{h_{r-s,s}\}_{1 \leq s \leq \tilde{\eta}}$ denote the missing data at time r . In the MCEM algorithm, N_0 denotes the Monte-Carlo sample size, and $Data_{miss,r}^{(m,k)}$, $1 \leq m \leq N_0$ denotes the m -th Monte-Carlo sample in the k -th iteration of the EM algorithm. Throughout the following, (k) denotes the k -th EM iteration. For example, $\gamma^{(k)}$ represents the current estimate of γ after the k -th EM iteration, with $R_r^{(k)}$ and $\Lambda_r^{(k)}$ representing estimates of R_r and Λ_r based on (2.1) and (2.4), using parameter values $\gamma^{(k)}$. The estimation procedure is outlined below, with a pseudo-code provided in Algorithm 1:

E step At the $(k+1)$ -th iteration, given the current estimate $\gamma^{(k)} = (\beta^{(k)}, \theta^{(k)}, \omega^{(k)}, \tilde{\omega}^{(k)})$, this step computes the expected complete data composite log-likelihood, or the Q-function:

$$Q(\gamma | \gamma^{(k)}) \stackrel{\text{def}}{=} \sum_{0 \leq r \leq t} \mathbb{E}_{\gamma^{(k)}} \left(\log \mathbb{P}_{\gamma} (H_r, I_r, Data_{miss,r} | \mathcal{F}_{r-1}) | Data_{obs,r} \right), \quad (3.10)$$

where the expectation is taken over the distribution of $Data_{miss,r}$ conditional on $(Data_{obs,r}, \gamma^{(k)})$.

Due to computational complexity, the Q-function is approximated using Monte Carlo sampling of $Data_{miss,r}$ from $\mathbb{P}_{\gamma^{(k)}}(Data_{miss,r} | Data_{obs,r})$, and is calculated as

$$\hat{Q}(\gamma | \gamma^{(k)}) \stackrel{\text{def}}{=} \sum_{0 \leq r \leq t} \frac{1}{N_0} \sum_{m=1}^{N_0} \log \mathbb{P}_{\gamma} (H_r, I_r, Data_{miss,r}^{(m,k)} | \mathcal{F}_{r-1}).$$

M step This step is to compute $\gamma^{(k+1)} = \arg \max_{\gamma \in \Gamma} \hat{Q}(\gamma | \gamma^{(k)})$. If $\arg \max_{\gamma \in \Gamma} \hat{Q}(\gamma | \gamma^{(k)})$ is not unique, we randomly choose one as $\gamma^{(k+1)}$. When $\hat{Q}(\gamma^{(k)} | \gamma^{(k)}) = \max_{\gamma \in \Gamma} \hat{Q}(\gamma | \gamma^{(k)})$, we choose $\gamma^{(k+1)} = \gamma^{(k)}$.

Notably, drawing samples from $P_{\gamma^{(k)}}(Data_{miss,r} | Data_{obs,r})$ is equivalent to sampling from $P_{\gamma^{(k)}}(H_r, I_r, Data_{miss,r} | \mathcal{F}_{r-1})$, as $P_{\gamma^{(k)}}(H_r, I_r | \mathcal{F}_{r-1})$ in equation (2.9) is constant for a given $\gamma^{(k)}$. To improve sampling efficiency, we use an acceptance-rejection method in Algorithm 1.

Specifically, samples are first drawn from $P_{\gamma^{(k)}}(Data_{miss,r} | \mathcal{F}_{r-1})$ and accepted with probability $p_{acceptance}$, proportional to $P_{\gamma^{(k)}}(H_r, I_r | Data_{miss,r}, \mathcal{F}_{r-1})$, where $\max_{H_r, I_r} p_{acceptance} \leq 1$. To further enhance efficiency, particularly when infections and hospitalizations are large ($H_t \geq 25$) in later pandemic stages, $p_{acceptance}$ in Algorithm 1 can be adjusted using Stirling's approximation:

$$p_{acceptance-adj} = 2\pi R_r^{(k)} \Lambda_r^{(k)} \sqrt{\tilde{\omega}_0^{(k)}(1 - \tilde{\omega}_0^{(k)})} p_{acceptance}.$$

Algorithm 1 An MCEM algorithm to estimate model parameters with unknown ω_s and $\tilde{\omega}_s$.

Require: initial parameter value $\gamma^{(0)}$, $k \leftarrow 0$, breakpoint critical value Δ_0 .

while $\|\gamma^{(k+1)} - \gamma^{(k)}\|_\infty > \Delta_0$, **set** $r \leftarrow 0$, $m \leftarrow 1$, **do**

while $0 \leq r \leq t$, $1 \leq m \leq N_0$, **do**

 Sample $h_{r-s,s}$ independently from $\text{Binomial}(I_{r-s}, \tilde{\omega}_s^{(k)})$, for $1 \leq s \leq \tilde{\eta}$.

 Sample ψ from Bernoulli distribution with probability $p_{acceptance}$, where

$$\begin{aligned} p_{acceptance} &= \mathbb{P}\left(Poisson(\tilde{\omega}_0^{(k)} R_r^{(k)} \Lambda_r^{(k)}) = H_r - \sum_{s=1}^{\tilde{\eta}} h_{r-s,s}\right) \\ &\times \mathbb{P}\left(Poisson((1 - \tilde{\omega}_0^{(k)}) R_r^{(k)} \Lambda_r^{(k)}) = I_r - H_r + \sum_{s=1}^{\tilde{\eta}} h_{r-s,s}\right) \end{aligned}$$

if $\psi = 1$, **then**

 let $Data_{miss,r}^{(m,k)} = \{h_{r-s,s}\}_{1 \leq s \leq \tilde{\eta}}$, $m \leftarrow m + 1$.

end if

if $m > N_0$, **then**

 let $r \leftarrow r + 1$, $m \leftarrow 1$.

end if

end while

Calculate the Monte Carlo Q-function $\hat{Q}(\gamma | \gamma^{(k)})$ and $\gamma^{(k+1)} = \arg \max_{\gamma \in \Gamma} \hat{Q}(\gamma | \gamma^{(k)})$.

Let $k \leftarrow k + 1$, $\hat{\gamma} \leftarrow \gamma^{(k+1)}$.

end while

Output $\hat{\gamma}$.

In Algorithm 1, the parameters of the infectiousness function, ω_s , and hospitalization propen-

sity, $\tilde{\omega}_s$, are assumed to be unknown. This scenario is often encountered in the early stages of novel pandemics when little is known about the infectious pathogens. However, prior knowledge about ω_s and $\tilde{\omega}_s$ may sometimes be available from multiple biomedical or contact tracing studies. In such scenarios, we may consider these estimates from other studies as prior knowledge. In the Supplementary Materials, we provide another MCEM algorithm, Algorithm 2, to estimate the model parameters when prior knowledge about ω_s and $\tilde{\omega}_s$ is available.

3.2 Asymptotic Properties

The basic TSI model (2.1), which describes the generative nature of an infectious pathogen, shares similarities with a branching process. Since branching process degenerates on an extinction set with no asymptotic properties, we similarly define an extinction set \mathcal{E} for the TSI model,

$$\mathcal{E} \stackrel{\text{def}}{=} \left\{ I_r = 0, \text{ for } r \text{ greater than some } K \right\} = \bigcup_{r \geq 1} \left\{ \frac{\partial \log \mathbb{P}(I_r, H_r | \mathcal{F}_{r-1})}{\partial \gamma} = 0 \right\}, \quad (3.11)$$

and define $\mathcal{E}_{\text{none}} = \mathcal{E}^c$. Often, no consistent estimator $\hat{\gamma}$ exists in \mathcal{E} . Thus, we set aside the extinction probability

$$\mathbb{P}(\mathcal{E}) = \mathbb{P}\left(\bigcup_{r \geq 1} \left\{ \frac{\partial \log \mathbb{P}(I_r, H_r | \mathcal{F}_{r-1})}{\partial \gamma} = 0 \right\}\right)$$

and focus on the asymptotic behavior of $\hat{\gamma}$ on the non-extinction set $\mathcal{E}_{\text{none}}$.

In the following theorems, we show that the proposed MCEM algorithm preserves the ascent property of the composite likelihood function and converges for our model. We then establish the consistency of the maximum composite likelihood estimator and present it in the practical form of Equation (2.4), under certain regularity conditions. Proof details are provided in the Supplementary Materials.

Theorem 1 (Ascent property of the composite likelihood) For $k \geq 0$, we have $\ell_C(\gamma^{(k+1)}) \geq \ell_C(\gamma^{(k)})$.

Theorem 2 (Convergence of the MCEM algorithm) Assume Γ is a compact set, then with $k \rightarrow \infty$,

the MCEM-estimator $\gamma^{(k)}$ at the k -th iteration converges to one of the stationary point γ_s induced by $M(\cdot) = \arg \max_{\gamma \in \Gamma} Q(\gamma \mid \cdot)$, and $\ell_C(\gamma^{(k)})$ converges monotonically to $\ell_C(\gamma_s)$.

To establish the consistency of the maximum composite likelihood estimator, we impose regularity conditions on the observed time series. Inspired by work on counting processes (Zeger and Qaqish, 1988; Davis *and others*, 1999, 2000, 2003), we assume:

Condition 1 (Series ergodicity) There exist $t_0 > 0$, such that,

$$\lim_{t \rightarrow \infty} \frac{t_0}{t} \sum_{s=1}^t R_s \Lambda_s \rightarrow_{a.s.} \sum_{s=1}^{t_0} \mathbb{E} R_s \Lambda_s, \quad \lim_{t \rightarrow \infty} \frac{t_0}{t} \sum_{s=1}^t I_s \log(R_s) \rightarrow_{a.s.} \sum_{s=1}^{t_0} \mathbb{E} I_s \log(R_s).$$

We also assume the time series regression in Equation (2.4) uses a log link function and follows an autoregressive model of order 1, such that $\log(R_t) = Z_t^T \beta + \theta_0 + \theta_1 \log(R_{t-1})$, where θ_0 is an intercept term extracted from both the exogenous terms and the autoregressive terms and θ_1 serves as the autoregressive parameter, capturing the dependence of R_t on its previous value. We then establish the consistency of the maximum composite likelihood estimator for the time series regression coefficients when the infectiousness function and hospitalization propensity, $(\omega_s, \tilde{\omega}_s)$, are known. We denote the parameters of interest as $\gamma|_{\omega} = (\beta, \theta)$. The consistency of the maximum composite likelihood estimator, $\hat{\gamma}|_{\omega} = (\hat{\beta}, \hat{\theta})$, is shown as follows.

Theorem 3 (Strong consistency of the estimators) Under condition 1 and assuming that Γ is a compact set, we have $\hat{\gamma}|_{\omega} \xrightarrow{a.s.} \gamma_0|_{\omega}$ as the length of the observational days $t \rightarrow \infty$, where $\gamma_0|_{\omega}$ is the parameter value corresponding to the true data generating mechanism.

Furthermore, with the following conditions from the theorem 3 of Kaufmann (1987), that is

Condition 2 (Non-singularity) For each $1 \leq r \leq t$, define

$$\xi_r(\gamma|_{\omega}) = \frac{\partial R_r}{\partial \gamma|_{\omega}} \cdot R_r^{-1} \cdot (I_r - R_r \Lambda_r).$$

There exists some nonrandom and non-singular normalizing matrix A_t , such that the normalized

conditional variance converges to an almost surely positive definite random matrix $\zeta^T \zeta$, i.e.,

$$A_t^{-1} \left[\sum_{r=1}^t \text{Cov}(\xi_r(\gamma_0|_\omega) | \mathcal{F}_{r-1}) \right] (A_t^{-1})^T \xrightarrow{P} \zeta^T \zeta.$$

Condition 3 (Uniformly integrability) For $1 \leq r \leq t$, $\mathbb{E}[\xi_r^2(\gamma_0) | \mathcal{F}_{r-1}]$ is termwise uniformly integrable.

Condition 4 (The conditional Lindeberg condition) For arbitrary $\epsilon > 0$,

$$\sum_{r=1}^t \mathbb{E} \left[\xi_r^T(\gamma_0|_\omega) (A_t^T A_t)^{-1} \xi_r(\gamma_0|_\omega) \cdot \mathbb{1}(|\xi_r^T(\gamma_0|_\omega) (A_t^T A_t)^{-1} \xi_r(\gamma_0|_\omega)| > \epsilon^2) | \mathcal{F}_{r-1} \right] \xrightarrow{P} 0.$$

Condition 5 (The smoothness condition) For arbitrary $\delta > 0$, and δ -neighborhood ball $\mathcal{B}_t(\delta)$ defined as $\mathcal{B}_t(\delta) = \{\tilde{\gamma}|_\omega : \|A_t^T(\tilde{\gamma}|_\omega - \gamma_0|_\omega)\| \leq \delta\}$,

$$\sup_{\tilde{\gamma}|_\omega \in \mathcal{B}_t(\delta)} \left\| A_t^{-1} \sum_{r=1}^t \left(\frac{\partial \xi_r(\tilde{\gamma}|_\omega)}{\partial \gamma} + \text{Cov}(\xi_r(\gamma_0|_\omega) | \mathcal{F}_{r-1}) \right) (A_t^{-1})^T \right\| \xrightarrow{P} 0.$$

the maximum composite likelihood estimator converges to a normal distribution as shown below.

Theorem 4 (Asymptotic normality) Under condition 1-5, and assume Γ is a compact set, then on the non-extinction set defined in (3.11), with $t \rightarrow \infty$,

$$\left[\sum_{r=1}^t \text{Cov}(\xi_r(\gamma_0|_\omega) | \mathcal{F}_{r-1}) \right]^{1/2} (\hat{\gamma}|_\omega - \gamma_0|_\omega) \xrightarrow{d} N(0, I), \quad (3.12)$$

where I is the identity matrix.

4. SIMULATION STUDIES

4.1 *Simulation Setups*

To evaluate the performance of the proposed method, we conducted simulation studies under two sets of scenarios. In the first, reported new infections represent the true counts, meaning the TSI model is correctly specified (correctly specified model). In the second, reported counts include errors (e.g., under-reporting or limited testing), implying the TSI model is misspecified (misspecified model). In both scenarios, hospitalization data were assumed accurate. Each scenario was

repeated 1,000 times to assess bias and coverage probability of the estimator.

Daily infections, hospitalizations, and covariates were generated from the proposed model (2.1)-(2.5), with a simplified form of (2.4): $\log(R_r) = Z_r^T \beta + \theta_0 + \theta_1 \log(R_{r-1})$, for $r \geq 1$, which means that the logarithm of the instantaneous reproduction number $\{R_r\}_{1 \leq r \leq t}$ follows an AR(1) structure with exogenous terms. Following Li *and others* (2020), the infectiousness function, approximated by the serial interval, was reported to follow a Gamma distribution with a mean of 7.5 days (95% CI: [5.3, 19]), corresponding to a standard deviation ranging from approximately 1.12 to 5.86. Our simulations used a Gamma distribution for the infectiousness function, with shape and scale parameters adjusted to mirror these results. Similarly, hospitalization propensity was set to a Gamma distribution to mimic the delay between disease onset and hospitalization reported in the same study:

$$\begin{aligned}\omega_s &= \mathbb{P}(\Gamma(k_1, \mu_1) \in [s-1, s]), \quad s = 1, \dots, 24, \quad \text{and} \quad \omega_{25} = \mathbb{P}(\Gamma(k_1, \mu_1) \geq 24), \\ 2\tilde{\omega}_s &= \mathbb{P}(\Gamma(k_2, \mu_2) \in [s, s+1]), \quad s = 0, \dots, 4, \quad 2\tilde{\omega}_5 = \mathbb{P}(\Gamma(k_2, \mu_2) \geq 5), \quad \text{and} \quad \tilde{\omega}_{-1} = 0.5,\end{aligned}$$

where $\Gamma(\cdot, \cdot)$ had shape parameters $\check{k}_1 = 2.5$, $\check{k}_2 = 1.6$, and scale parameters $\mu_1 = 3$, $\mu_2 = 1.5$. We set the study duration $T = 120$ and fixed $p = 2$. Parameter values were assigned as $(\theta_0, \theta_1, \beta^T) = (0.7, 0.5, -0.02, -0.125)$. We independently simulated two covariates $\{Z_{r,1}, Z_{r,2}\}_{1 \leq r \leq t}$ to mimic real data on temperature in Philadelphia and social distancing trends obtained from daily cellular telephone movements, as provided by Unacast (Unacast, July 1st). This data represented the percentage change in visits to non-essential businesses, such as restaurants and hair salons, between March 1st and June 30th, 2020.

4.2 Simulation Results with Correctly Specified Model

In this set of scenarios, we explored three circumstances and compared the proposed method to the reference approach by Cori *and others* (2013). In the first circumstance, we assumed the infectiousness function ω_s and hospitalization propensity $\tilde{\omega}_s$ were known. The model parame-

ters reduced to $\gamma = (\theta^T, \beta^T)$. For the reference approach, a 3-day sliding window was chosen by minimizing the \mathcal{L}_2 -distance between the estimated and oracle $\{R_r\}_{1 \leq r \leq t}$. Additional results for 1-day and 7-day windows are in the Supplementary Materials. For the proposed method, we selected the initial $\gamma^{(0)}$ randomly and away from the oracle value. Figure 2 shows both methods captured the trend of $\{R_r\}_{1 \leq r \leq t}$ well with very small estimation biases, but the proposed method performed better than the baseline method with a smaller bias. Moreover, when ω_s and $\tilde{\omega}_s$ were known, we found the proposed MCEM algorithm converged very fast, and the estimation bias for $\{R_r\}_{1 \leq r \leq t}$ reached its limit after only two iterations of running the algorithm. In the second circumstance, we assumed ω_s and $\tilde{\omega}_s$ were unknown but prior knowledge about ω_s was available. We used the estimated infectiousness functions from previous studies as the prior knowledge, (Wu and others, 2020; Ali and others, 2020; Chen and others, 2022; Deng and others, 2021), set the true function according to the results in Li and others (2020), and used Algorithm 2 to estimate the parameters. Results were similar to those observed in the first circumstance, except for a small increase in estimation bias for both methods. In the third circumstance, we assumed ω_s and $\tilde{\omega}_s$ were unknown and no prior knowledge was available. In this situation, we only estimated the parameters using the proposed method, since the reference approach either requires user-specified values to constrain the overall shape of the infectiousness function or needs user-provided contact tracking data to estimate the infectiousness function. Using the proposed method, we estimated the regression coefficients as well as the infectiousness function and hospitalization propensity. As shown in Table 1, the proposed method produced accurate estimates for parameters with small bias and good coverage probability. It also consistently estimated the instantaneous reproduction numbers (Figure S7 in Supplemental Materials). Overall, when the TSI model was correctly specified, the proposed composite likelihood MCEM algorithm benefited from incorporating hospital admission data, outperforming the reference approach.

4.3 *Simulation Results with Misspecified Model*

In the second set of scenarios, we assumed the reported daily new infections were inaccurate due to underreporting, with the proportion of reported cases varying daily. This reflects real-world challenges during the pandemic, where case reporting was influenced by testing availability, public compliance, and at-home testing. In contrast, hospitalization data were assumed accurate, as hospitals report admissions in standardized formats. Additional simulations involving underreporting of hospitalizations are included in the Supplementary Material.

Daily underreporting percentage was generated from a normal distribution with a mean of 15% and standard deviation of 5%. This allowed the daily under-reporting percentage to vary from 0% to 30%, resulting in poor data quality for the reported infection numbers. However, we assumed the daily hospital admission data were accurate, ensuring that all hospitalized patients were reported and documented in a timely manner. Using the oracle reproduction number, we simulated true infections, underreporting percentages, and hospitalizations for each replication. The proposed method produced results similar to the correctly specified model. For example, the mean point estimates for β in the mis-specified model (-0.0206, -0.1239) were nearly identical to those in the correctly specified model (-0.02, -0.125), though the standard errors were higher in the mis-specified scenario (0.003, 0.009) compared to the correctly specified model (0.0003, 0.0004). Compared to a recent measurement error model (Shi and others, 2022), the proposed method performed slightly better, providing more accurate estimates of the reproduction number (Figure 3).

5. APPLICATION TO COVID-19 DATA

We applied the proposed method to COVID-19 data from January 1 to June 30, 2021, for four major metropolitan counties: Miami-Dade, FL; New York, NY; Cook (Chicago), IL; and Wayne (Detroit), MI. These counties represent four major metropolitan areas in the Southeast coast,

Tri-State area, and Great Lakes region of the United States. County-level data on daily new infections and hospitalizations due to COVID-19 were obtained from the National Healthcare Safety Network (NHSN) database. Additionally, two county-level risk factors were sourced: daily social distancing practices, indicated by the percentage change in visits to nonessential businesses (from Unacast), and wet-bulb temperature (from the National Oceanic and Atmospheric Administration). These risk factors were selected based on a thorough review of the literature that has extensively examined local factors influencing COVID-19 transmission (Talic *and others*, 2021; Weaver *and others*, 2022; Rubin *and others*, 2020). Our objectives were to estimate the daily reproduction number R_t , infectiousness function ω_s , and hospitalization propensity $\tilde{\omega}_s$, and to assess the association between county-level factors and disease transmission. These findings aim to inform public health policies and resource allocation.

When fitting the proposed model, we allowed hospitalization propensity to vary by county to account for differences in healthcare resources and access. Due to limitations in US COVID-19 surveillance data, which recorded incidence at the time of disease diagnosis rather than actual infection, and considering that the exact infection times are rarely known, we interpreted the infectiousness function and hospitalization propensity estimated from this data based on diagnosis time rather than infection time. Specifically, $\tilde{\omega}_{-1,c}$ and $\tilde{\omega}_{s,c}$ represent the probabilities of never being hospitalized and being hospitalized on the s -th day after diagnosis, respectively, for each county $c \in 1, 2, 3, 4$. This approach captures county-level heterogeneity, while ω_s reflects infectiousness on the s -th day post-diagnosis. Bootstrap confidence intervals (CIs) were computed using the block approach (Bühlmann and Künsch, 1999). The time series structure (2.4) was selected via AIC from a family of autoregressive models with exogenous terms, and the lengths of the infectiousness function and hospitalization propensity (η and $\tilde{\eta}$) were determined by maximizing the composite likelihood.

The final model selected was the same AR(1) structure used in the simulation study, with η

and $\tilde{\eta}$ estimated at 22 and 4, respectively. The estimated effect sizes were 0.1539 (95% CI: 0.1537 to 0.1541) for social distancing and -7.3×10^{-4} (95% CI: -8.3×10^{-4} to -6.4×10^{-4}) for temperature, respectively. These results suggested that lack of social distancing was a strong risk factor for elevated disease transmission during the study period. For example, a 50% reduction in the frequency of visiting non-essential businesses was estimated to reduce R_t by an average of 7.4%. On the contrary, temperature exerted only a minor effect on disease transmission. The estimated county-level R_t exhibited a similar trend during the study period among all four counties, as depicted in Figure S8. A decrease in disease transmission was observed since April 2021, which, in this dataset, was largely attributed to a reduction in social distancing value. Figure S9 illustrates the estimated infectiousness function. Its shape resembled the probability density function of either a Gamma or Weibull distribution (Figure S9a), with nearly two-thirds of secondary infections being diagnosed within the first week after the diagnosis of the infectors (Figure S9b). If we assume that the duration between infection and diagnosis is roughly the same for both infectors and secondary infections, our finding suggests that timely testing and a subsequent week-long quarantine of infected individuals can significantly mitigate disease transmission. The estimated hospitalization propensity for each county is presented in Figure 4. Given the varied access to healthcare, hospitalization propensity diverged across locations. New York exhibited the highest propensity for hospitalization post-diagnosis (just under 20%), compared to about 10% in Miami. Hospitalization on the first day of diagnosis was also highest in New York (15.5%) but below 5% in Miami and Cook (Figure 4a). Across counties, most hospitalizations occurred within 4 days of diagnosis, with an average of 1 day from diagnosis to admission. Assuming a 48-hour delay from symptom onset to diagnosis, most hospitalizations occurred within 6 days of symptom onset, with a mean time to admission of approximately 3 days. These findings align with prior studies. For example, a CDC report estimated that 20.9% of U.S. COVID-19 patients were hospitalized before March 28, 2020 (Team and others, 2020). Zhang and others (2020) found a decrease in

mean time from symptom onset to admission in Hubei, China, from 4.4 days (Dec 24–Jan 27, 2019) to 2.6 days (Jan 28–Feb 17, 2020). Traditionally, studying such durations requires epidemiological studies with contact tracing data, which poses a high requirement for the US disease surveillance system. Our results demonstrate that, even without extensive contact tracing, U.S. surveillance data can be effectively leveraged to estimate critical parameters for hospital planning and outbreak response.

6. DISCUSSION

This study introduces a new model and estimation procedure that extends traditional TSI models by incorporating data augmentation for both incidence and hospitalization data, enabling more accurate estimation of the instantaneous reproduction number, especially when hospitalization data is more reliable than incidence data. Our model also facilitates estimating hospitalization propensity, previously achievable only through contact tracing, and assessing the association between risk factors and transmission dynamics. The model is broadly applicable where both incidence and hospitalization data are available, particularly when incidence data quality is low.

The proposed method offers several extension opportunities. First, it can incorporate additional data, such as daily death counts, PCR tests, and serological data, to improve parameter accuracy and model death counts. Second, spatial correlations in disease transmission could be added using traffic data to enhance model efficiency. Third, the model can accommodate evolving pathogen dynamics and immunity changes, enabling analysis of new virus variants and immunity impacts. Fourth, it could be adjusted to handle overdispersion in infection counts by using distributions like the negative binomial, as illustrated in the supplementary materials. Finally, while the algorithm’s runtime is manageable (1.7 to 6.5 minutes compared to 0.06 minutes in Cori *and others* (2013)), further optimization could improve efficiency.

In addition to these extensions, the selection of appropriate risk factors is critical for applying our method effectively. In our study, we identified relevant factors through a systematic

literature review and consultations with domain experts, focusing on those that significantly influence COVID-19 transmission dynamics. This approach ensured that the model captures local variations in transmission and improves the accuracy of R_t estimation. Including irrelevant variables could introduce noise and bias, undermining the model's performance. To assist users in selecting relevant factors in practice, we propose the following practical guidelines: 1) conduct a comprehensive literature review and consult with domain experts to identify strong candidate risk factors; 2) ensure the availability of reliable data and assess the correlation between potential risk factors and R_t ; 3) void multicollinearity and focus on variables that are most relevant to R_t .

7. SOFTWARE

Software in the form of R code, together with a sample example for the simulation study and complete documentation for the COVID-19 application is available on <https://github.com/Jiasheng-Shi/Infectious-Disease-Hospitalization>. Additional requests for implementation can be directed to the corresponding author at jing14@pennmedicine.upenn.edu.

8. SUPPLEMENTARY MATERIAL

Supplementary material is available online at <http://biostatistics.oxfordjournals.org>.

ACKNOWLEDGMENTS

Funding for the project was provided by the NIH under award R01HD099348 and CDC under award U01CK000674. *Conflict of Interest:* None declared.

REFERENCES

ABBOTT, SAM, THOMPSON, JAMES, FUNK, SEBASTIAN, HELLEWELL, JOEL AND EPIFORECASTS. (2021). *EpiNow2: Estimate real-time case counts and time-varying epidemiological parameters*. R package version 1.3.2.

ALI, SHEIKH TASLIM, WANG, LIN, LAU, ERIC HY, XU, XIAO-KE, DU, ZHANWEI, WU, YE, LEUNG, GABRIEL M AND COWLING, BENJAMIN J. (2020). Serial interval of SARS-CoV-2 was shortened over time by nonpharmaceutical interventions. *Science* **369**(6507), 1106–1109.

ATHREYA, KRISHNA B, NEY, PETER E AND NEY, PE. (2004). *Branching processes*. Courier Corporation.

BÜHLMANN, PETER AND KÜNSCH, HANS R. (1999). Block length selection in the bootstrap for time series. *Computational Statistics & Data Analysis* **31**(3), 295–310.

CHEN, DONGXUAN, LAU, YIU-CHUNG, XU, XIAO-KE, WANG, LIN, DU, ZHANWEI, TSANG, TIM K, WU, PENG, LAU, ERIC HY, WALLINGA, JACCO, COWLING, BENJAMIN J and others. (2022). Inferring time-varying generation time, serial interval, and incubation period distributions for COVID-19. *Nature Communications* **13**(1), 7727.

CORI, ANNE. (2021). *EpiEstim: Estimate time varying reproduction numbers from epidemic curves*. R package version 2.2-4.

CORI, ANNE, FERGUSON, NEIL M, FRASER, CHRISTOPHE AND CAUCHEMEZ, SIMON. (2013). A new framework and software to estimate time-varying reproduction numbers during epidemics. *American Journal of Epidemiology* **178**(9), 1505–1512.

DAVIS, RICHARD A, DUNSMUIR, WILLIAM TM AND STREETT, SARAH B. (2003). Observation-driven models for poisson counts. *Biometrika* **90**(4), 777–790.

DAVIS, RICHARD A, DUNSMUIR, WILLIAM TM AND WANG, YING. (1999). Modeling time series of count data. *Statistics Textbooks and Monographs* **158**, 63–114.

DAVIS, RICHARD A, DUNSMUIR, WILLIAM TM AND WANG, YIN. (2000). On autocorrelation in a poisson regression model. *Biometrika* **87**(3), 491–505.

DENG, YUHAO, YOU, CHONG, LIU, YUKUN, QIN, JING AND ZHOU, XIAO-HUA. (2021). Estimation of incubation period and generation time based on observed length-biased epidemic cohort with censoring for covid-19 outbreak in china. *Biometrics* **77**(3), 929–941.

FRASER, CHRISTOPHE. (2007). Estimating individual and household reproduction numbers in an emerging epidemic. *PloS one* **2**(8), e758.

GE, YONG, WU, XILIN, ZHANG, WENBIN, WANG, XIAOLI, ZHANG, DIE, WANG, JIANGHAO, LIU, HAIYAN, REN, ZHOUPENG, RUKTANONCHAI, NICK W, RUKTANONCHAI, CORRINE W and others. (2023). Effects of public-health measures for zeroing out different sars-cov-2 variants. *Nature Communications* **14**(1), 5270.

GOSTIC, KATELYN M, MCGOUGH, LAUREN, BASKERVILLE, EDWARD B, ABBOTT, SAM, JOSHI, KEYA, TEDIJANTO, CHRISTINE, KAHN, REBECCA, NIEHUS, RENE, HAY, JAMES A, DE SALAZAR, PABLO M and others. (2020). Practical considerations for measuring the effective reproductive number, R_t . *PLoS Computational Biology* **16**(12), e1008409.

GRESSANI, OSWALDO, WALLINGA, JACCO, ALTHAUS, CHRISTIAN L, HENS, NIEL AND FAES, CHRISTEL. (2022). Epilps: A fast and flexible bayesian tool for estimation of the time-varying reproduction number. *PLoS computational biology* **18**(10), e1010618.

JEWELL, NICHOLAS P. (2021). Statistical models for covid-19 incidence, cumulative prevalence, and r t. *Journal of the American Statistical Association* **116**(536), 1578–1582.

KAUFMANN, HEINZ. (1987). Regression models for nonstationary categorical time series: asymptotic estimation theory. *The Annals of Statistics*, 79–98.

KERMACK, WILLIAM OGILVY AND MCKENDRICK, ANDERSON G. (1927). A contribution to the mathematical theory of epidemics. *Proceedings of the royal society of london. Series A, Containing papers of a mathematical and physical character* **115**(772), 700–721.

LI, QUN, GUAN, XUHUA, WU, PENG, WANG, XIAOYE, ZHOU, LEI, TONG, YEQING, REN, RUIQI, LEUNG, KATHY SM, LAU, ERIC HY, WONG, JESSICA Y *and others*. (2020). Early transmission dynamics in Wuhan, China, of novel coronavirus–infected pneumonia. *New England Journal of Medicine*.

LINDSAY, BRUCE. (1988). Composite likelihood methods. *Contemporary Mathematics* **80**, 220–239.

LLOYD-SMITH, JAMES O, SCHREIBER, SEBASTIAN J, KOPP, P EKKEHARD AND GETZ, WAYNE M. (2005). Superspreading and the effect of individual variation on disease emergence. *Nature* **438**(7066), 355–359.

NASH, REBECCA K, NOUVELLET, PIERRE AND CORI, ANNE. (2022). Real-time estimation of the epidemic reproduction number: Scoping review of the applications and challenges. *PLOS Digital Health* **1**(6), e0000052.

PAN, AN, LIU, LI, WANG, CHAOLONG, GUO, HUAN, HAO, XINGJIE, WANG, QI, HUANG, JIAO, HE, NA, YU, HONGJIE, LIN, XIHONG *and others*. (2020). Association of public health interventions with the epidemiology of the covid-19 outbreak in wuhan, china. *Jama* **323**(19), 1915–1923.

QUICK, CORBIN, DEY, ROUNAK AND LIN, XIHONG. (2021). Regression models for understanding covid-19 epidemic dynamics with incomplete data. *Journal of the American Statistical Association* **116**(536), 1561–1577.

ROSS, RONALD. (1916). An application of the theory of probabilities to the study of a priori pathometry.—Part I. *Proceedings of the Royal Society of London. Series A, Containing Papers of a Mathematical and Physical Character* **92**(638), 204–230.

ROSS, RONALD AND HUDSON, HILDA P. (1917a). An application of the theory of probabilities

to the study of a priori pathometry.—Part II. *Proceedings of the Royal Society of London. Series A, Containing Papers of a Mathematical and Physical Character* **93**(650), 212–225.

Ross, RONALD AND HUDSON, HILDA P. (1917b). An application of the theory of probabilities to the study of a priori pathometry.—Part III. *Proceedings of the Royal Society of London. Series A, Containing Papers of a Mathematical and Physical Character* **93**(650), 225–240.

RUBIN, DAVID, HUANG, JING, FISHER, BRIAN T, GASPARRINI, ANTONIO, TAM, VICKY, SONG, LIHAI, WANG, XI, KAUFMAN, JASON, FITZPATRICK, KATE, JAIN, ARUSHI *and others*. (2020). Association of social distancing, population density, and temperature with the instantaneous reproduction number of SARS-CoV-2 in counties across the United States. *JAMA Network Open* **3**(7), e2016099–e2016099.

SHI, JIASHENG, MORRIS, JEFFREY S, RUBIN, DAVID M AND HUANG, JING. (2022). Robust modeling and inference of disease transmission using error-prone data with application to sars-cov-2. *arXiv preprint arXiv:2212.08282*.

SVENSSON, ÅKE. (2007). A note on generation times in epidemic models. *Mathematical Biosciences* **208**(1), 300–311.

TALIC, STELLA, SHAH, SHIVANGI, WILD, HOLLY, GASEVIC, DANIJELA, MAHARAJ, ASHIKA, ADEMI, ZANFINA, LI, XUE, XU, WEI, MESA-EGUIAGARAY, INES, ROSTRON, JASMIN *and others*. (2021). Effectiveness of public health measures in reducing the incidence of COVID-19, SARS-CoV-2 transmission, and COVID-19 mortality: systematic review and meta-analysis. *BMJ* **375**.

TEAM, CDC COVID-19 RESPONSE, TEAM, CDC COVID-19 RESPONSE, TEAM, CDC COVID-19 RESPONSE, CHOW, NANCY, FLEMING-DUTRA, KATHERINE, GIERKE, RYAN, HALL, ARON, HUGHES, MICHELLE, PILISHVILI, TAMARA, RITCHEY, MATTHEW *and others*. (2020). Preliminary estimates of the prevalence of selected underlying health conditions

among patients with coronavirus disease 2019—United States, February 12–March 28, 2020. *Morbidity and Mortality Weekly Report* **69**(13), 382–386.

UNACAST. Social distancing scoreboard.

VARIN, CRISTIANO, REID, NANCY AND FIRTH, DAVID. (2011). An overview of composite likelihood methods. *Statistica Sinica*, 5–42.

WALLINGA, JACCO AND TEUNIS, PETER. (2004). Different epidemic curves for severe acute respiratory syndrome reveal similar impacts of control measures. *American Journal of Epidemiology* **160**(6), 509–516.

WEAVER, AMANDA K, HEAD, JENNIFER R, GOULD, CARLOS F, CARLTON, ELIZABETH J AND REMAIS, JUSTIN V. (2022). Environmental factors influencing COVID-19 incidence and severity. *Annual Review of Public Health* **43**(1), 271–291.

WHO EBOLA RESPONSE TEAM. (2014). Ebola virus disease in West Africa—the first 9 months of the epidemic and forward projections. *New England Journal of Medicine* **371**(16), 1481–1495.

WU, JOSEPH T, LEUNG, KATHY, BUSHMAN, MARY, KISHORE, NISHANT, NIEHUS, RENE, DE SALAZAR, PABLO M, COWLING, BENJAMIN J, LIPSITCH, MARC AND LEUNG, GABRIEL M. (2020). Estimating clinical severity of COVID-19 from the transmission dynamics in Wuhan, China. *Nature Medicine* **26**(4), 506–510.

ZEGER, SCOTT L AND QAQISH, BAHJAT. (1988). Markov regression models for time series: a quasi-likelihood approach. *Biometrics*, 1019–1031.

ZHANG, JUANJUAN, LITVINOVA, MARIA, WANG, WEI, WANG, YAN, DENG, XIAOWEI, CHEN, XINGHUI, LI, MEI, ZHENG, WEN, YI, LAN, CHEN, XINHUA and others. (2020). Evolving epidemiology and transmission dynamics of coronavirus disease 2019 outside Hubei province, China: a descriptive and modelling study. *The Lancet Infectious Diseases* **20**(7), 793–802.

Table 1. Performance of the proposed method when the reported number of daily new infections was accurate, the infectiousness function ω_s and hospitalization propensity $\tilde{\omega}_s$ were unknown and no prior knowledge was available. For ω_s and $\tilde{\omega}_s$, only estimates of selected parameters are presented, due to the large number of parameters. Estimates of the other parameters not shown here yield similar results.

	θ_0	θ_1	β_1	β_2	ω_5	ω_6	$\tilde{\omega}_0$
Empirical bias ($\times 10^{-3}$)	-0.15	2.10	0.08	0.15	-0.45	-0.40	-0.04
Relative bias ($\times 10^{-3}$)	-0.22	4.20	-3.79	-1.23	-4.40	-4.01	-0.32
Standard error ($\times 10^{-3}$)	6.29	3.34	0.23	0.39	2.23	2.29	0.60
95% Coverage probability	94.6%	92.0%	94.2%	96.2%	96.2%	97.0%	94.4%

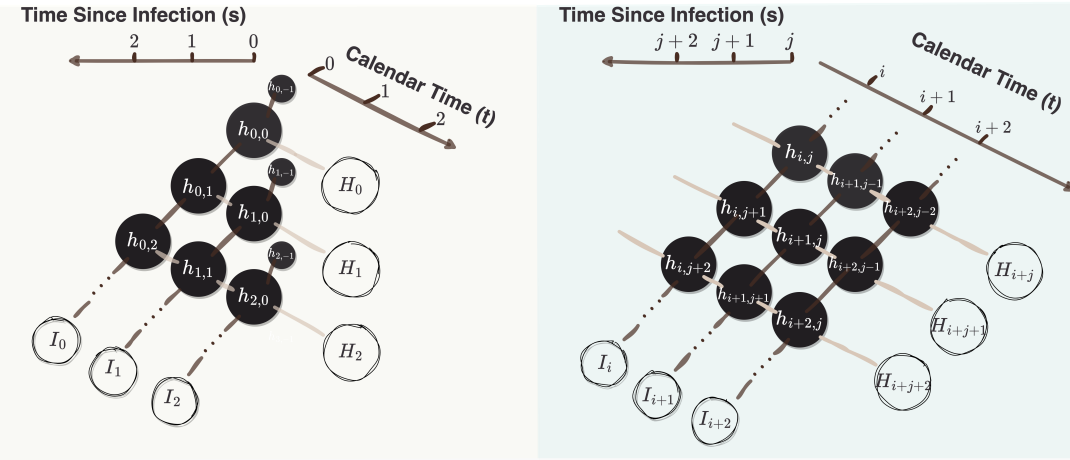


Fig. 1. The relationship between incidence data I_t and hospitalization data H_t . The left panel illustrates the relationship between calendar time 0 and 2 and time since infection from 0 to 2. The right panel illustrates the relationship between calendar time i and $i + 2$ and time since infection from j to $j + 2$.

[Received August 1, 2010; revised October 1, 2010; accepted for publication November 1, 2010]

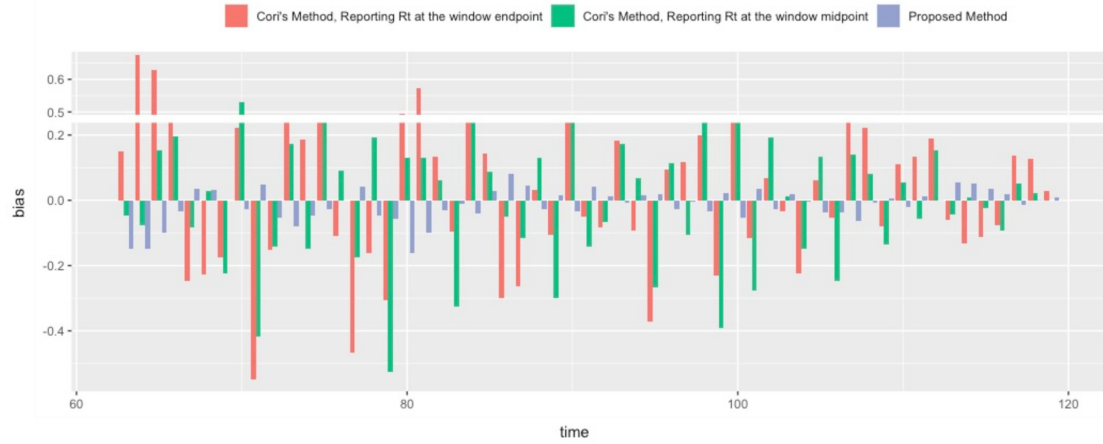


Fig. 2. Comparison of the estimation bias in the daily instantaneous reproduction number, R_t , between the proposed method, Cori's method that reports R_t at the endpoint of the sliding window (Cori and others, 2013), and Cori's method that reports R_t at the midpoint of the sliding window (Gostic and others, 2020; Gressani and others, 2022), when the reported number of daily new infections was accurate, and both the infectiousness function ω_s and hospitalization propensity $\tilde{\omega}_s$ were known. For the reference approach, a three days sliding window is selected by minimizing the \mathcal{L}_2 -distance of the estimated and oracle sequence of $\{R_r\}_{1 \leq r \leq t}$, and a comparison to reference approach with different sliding window is left to the supplementary. The estimation bias was calculated as the difference between the estimated daily R_t and the oracle R_t that generates the data. The bias is plotted starting from day 60, as Cori and others (2013) demonstrated substantial bias and unstable estimation during the early stages of the simulated period when the incident cases I_t were small ($\leq 2 \times 10^3$).

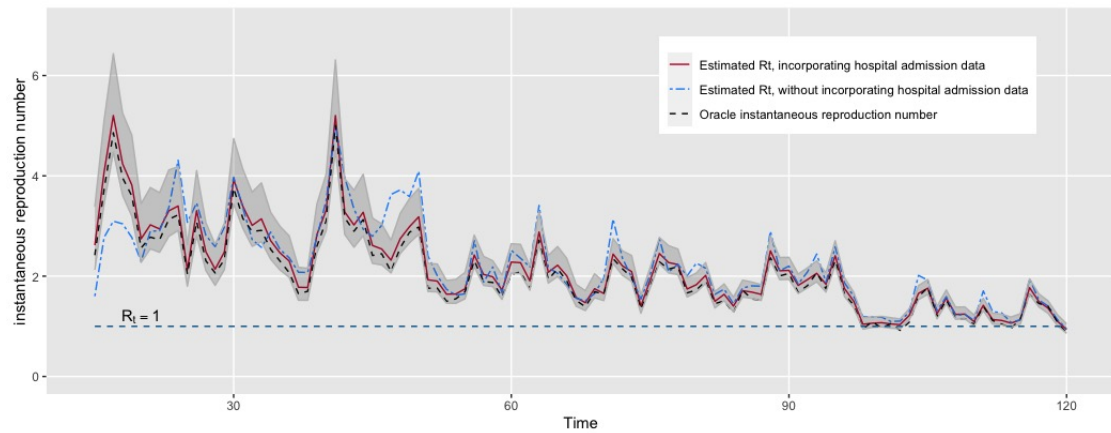


Fig. 3. Estimation of the instantaneous reproduction number when the daily new infections were reported with 0%-30% under-reporting rates. Black dotted line stands for the oracle instantaneous reproduction number. Red solid line and the gray shadow stand for the estimates and its corresponding Bootstrapping confidence interval (90% confidence level) using the proposed method. Blue dashed line stands for the estimates using a comparison method (Shi *and others*, 2022).

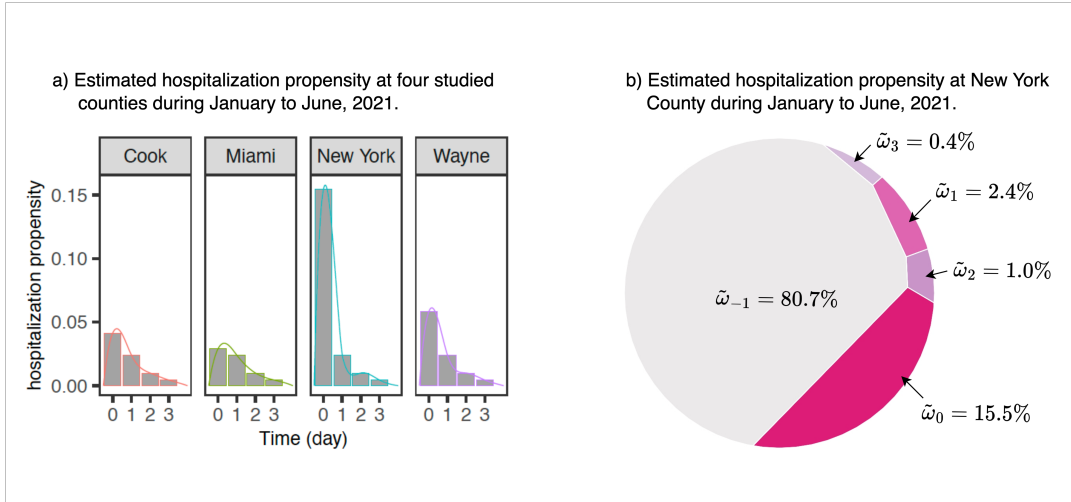


Fig. 4. Visualization of the estimated hospitalization propensity, $\tilde{\omega}_s$, for COVID-19 in the four studied counties during February to May 2021. In panel a), the bar plot shows the estimated value of $\tilde{\omega}_s$, $1 \leq s \leq 4$, at the four studied counties, while the solid lines represent the estimated propensity after fitting a cubic smoothing spline. In panel b), the estimated $\tilde{\omega}_s$ values at New York County are visualized using a Voronoi diagram to compare the magnitude of each $\tilde{\omega}_s$. Most of the hospitalized patients were admitted to a hospital on the day of infection.

Time-Since-Infection Model for Hospitalization and Incidence Data

SUPPLEMENTARY MATERIALS

The Supplementary Materials include the following sections: (i) a general model setting where $D_{2,t}$ in (5) is replaced with $\{I_r, H_r\}_{0 \leq r \leq t-1}$, along with its corresponding simulation performance; (ii) an extension of the model to account for overdispersion in daily infection counts; (iii) Algorithm 2, an MCEM algorithm for parameter estimation when prior knowledge of ω and ω_s is available; (iv) additional clarification on the simulation setup; (v) a comparison of the estimated R_t with that of [Cori et al. \(2013\)](#) using various sliding window lengths; (vi) simulations addressing underreported incidence and hospitalization data; (vii) detailed proofs of all technical results; and (viii) additional results from the simulation study and application to COVID-19 Data.

I General model setting and corresponding simulation

Consider the general setting in which we replace $D_{2,t}$ in (4) and (5) with $\{I_j, H_j\}_{0 \leq j \leq t-1}$, denoted as $D'_{2,t}$. Since $D'_{2,t} \subset \mathcal{G}_t$, we will first make adjustment to the base layer of the TSI model in Equation (1) to

$$I_t | \mathcal{G}_{t-1} \sim \text{Poisson}(R_t \Lambda_t), \quad \text{with } \Lambda_t = \sum_{1 \leq s \leq t} \omega_s I_{t-s}. \quad (12)$$

In most cases (with the general formula in Equation (4)), the joint likelihood and composite likelihood become intractable due to the irregular range restriction of $H_r | \mathcal{G}_{r-1}$. However, for a special case of Equation (4) where R_t depends on $D'_{2,t}$ only through $\{H_{t-1}\} \cup \mathcal{F}_t$, and R_t is independent of $\{H_{t-2}, \dots, H_0\}$, e.g.,

$$\log(R_t) - \theta_1 \log(H_{t-1}/I_{t-1}) = Z_t^T \beta + \theta_2 \left[\log(R_{t-1}) - \theta_1 \log(H_{t-2}/I_{t-2}) \right]. \quad (13)$$

In practice, the term involving H_{t-1}/I_{t-1} can be interpreted as the effect brought by quarantine or similar interventions, and we obtain the composite likelihood

$$\begin{aligned} \ell_C &= \sum_{0 \leq r \leq t} \log \mathbb{P}(H_r, I_r | \mathcal{F}_{r-1}) \\ &= \sum_{0 \leq r \leq t} \log \mathbb{P}(H_r | \mathcal{F}_r) \cdot \mathbb{P}(I_r | \mathcal{F}_{r-1}) \\ &= \sum_{0 \leq r \leq t} \log \mathbb{P}(H_r | \mathcal{F}_r) + \sum_{0 \leq r \leq t} \log \sum_{\ddot{H}_{r-1}} \mathbb{P}(I_r | \ddot{H}_{r-1}, \mathcal{F}_{r-1}) \cdot \mathbb{P}(\ddot{H}_{r-1} | \mathcal{F}_{r-1}). \end{aligned}$$

Notice that $\mathbb{P}(I_r | \ddot{H}_{r-1}, \mathcal{F}_{r-1})$ is a Poisson distribution function. For each $0 \leq r \leq t$,

$$\mathbb{P}(\ddot{H}_r | \mathcal{F}_r) = \sum_{h_{r-\tilde{\eta}, \tilde{\eta}}, \dots, h_{r-1, 1}} \mathbb{P}\left(h_{r,0} = (\ddot{H}_r - \sum_{s=1}^{\tilde{\eta}} h_{r-s,s}), h_{r-s,s}, 1 \leq s \leq \tilde{\eta} | \mathcal{F}_r\right)$$

$$\begin{aligned}
&= \sum_{h_{r-\tilde{\eta}, \tilde{\eta}}, \dots, h_{r-1,1}} \mathbb{P}\left(\text{Binomial}(I_r, \tilde{\omega}_0) = (\ddot{H}_r - \sum_{s=1}^{\tilde{\eta}} h_{r-s,s})\right) \\
&\quad \cdot \prod_{s=1}^{\tilde{\eta}} \mathbb{P}\left(\text{Binomial}(I_{r-s}, \tilde{\omega}_s) = h_{r-s,s}\right).
\end{aligned}$$

We conduct a simulation using the general setting model, where we set the infectiousness function and the hospitalization propensity as

$$\begin{aligned}
\omega &= (0.27, 0.29, 0.17, 0.12, 0.09, 0.06), \text{ with } \eta = 6, \\
\text{and } \tilde{\omega} &= (\tilde{\omega}_{-1} = 0.85, \tilde{\omega}_0 = 0.1, \tilde{\omega}_1 = 0.05), \text{ with } \tilde{\eta} = 2.
\end{aligned}$$

We further set the number of infections, hospitalizations, and the instantaneous reproduction number at time zero to be 50, 7 and 2.5, respectively. The simulated study period lasts for $T = 120$ days, and the maximum daily incidence is below 500. We incorporate two covariates, social distancing and wet-bulb temperature, directly from the New York County data used in Section 4 of the main manuscript, covering the period from January 1st to April 30th, 2021, with covariate effects being $(0.25, -0.01)$. We estimate the model parameters and the instantaneous reproduction number over time and compare them to the true values. The results are similar to those shown in the simulation section of the main manuscript. We also demonstrate the estimated instantaneous reproduction number from one randomly selected replicate in Figure S1.

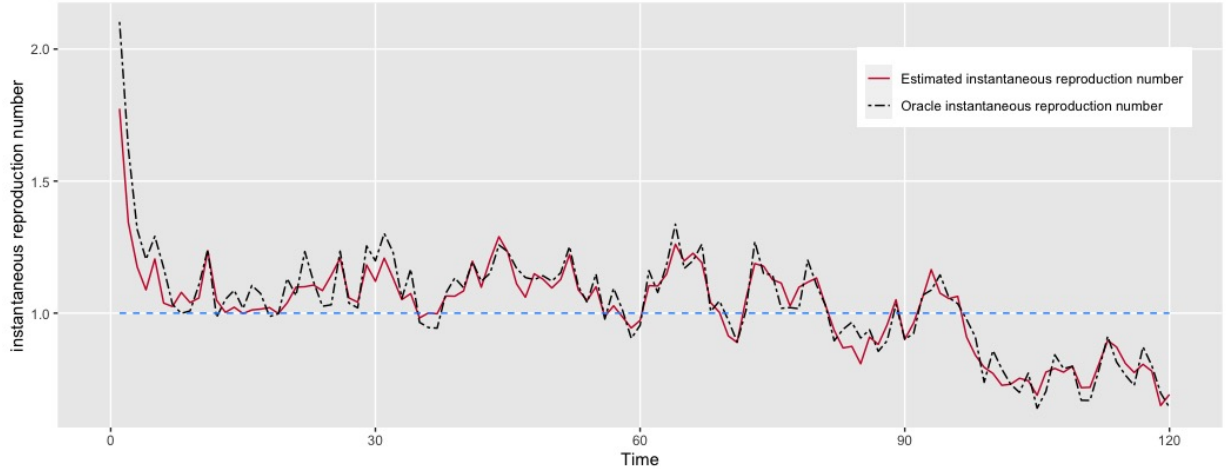


Figure S1: The estimated instantaneous reproduction number from one randomly selected replicate using data simulated from the general setting model.

II Model extention: overdispersion in daily infection numbers

The proposed approach is applicable to distributions with an overdispersion parameter. However, the composite likelihood functions need to be adjusted on a case-by-case basis. For example, when $I_t | \mathcal{F}_{t-1}$ is assumed to follow a negative binomial distribution, i.e.,

$$\mathbb{P}(I_t | \mathcal{F}_{t-1}) = \frac{\Gamma(I_t + \Lambda_t R_t)}{\Gamma(R_t \Lambda_t) I_t!} (1-p)^{I_t} p^{R_t \Lambda_t},$$

the composite likelihood (2.8) in our manuscript needs to be updated accordingly. Conditional on $\mathcal{F}_{t-1} \triangleq \sigma\{I_s, s \leq t-1\}$,

$$\begin{aligned}
& \mathbb{P}(H_t, I_t, h_{t-\eta, \eta}, \dots, h_{t-1, 1} | \mathcal{F}_{t-1}) \\
&= \mathbb{P}\left(h_{t-\eta, \eta}, \dots, h_{t-1, 1}, h_{t, 0} = H_t - \sum_{s=1}^{\eta} h_{t-s, s}, \right. \\
&\quad \left. \sum_{s=-1, 1, \dots, \eta} h_{t, s} = I_t - H_t + \sum_{s=1}^{\eta} h_{t-s, s} | \mathcal{F}_{t-1}\right) \\
&= \prod_{s=1}^{\eta} \mathbb{P}\left(\text{Binomial}(I_{t-s}, \tilde{\omega}_s)\right) \cdot \mathbb{1}\left(H_t - I_t \leq \sum_{s=1}^{\eta} h_{t-s, s} \leq H_t\right) \\
&\quad \times \mathbb{P}\left(\text{Multinomial}\left(I_t + R_t \Lambda_t ; \tilde{\omega}_0(1-p), (1-\tilde{\omega}_0)(1-p), p\right)\right. \\
&\quad \left.= \left(h_{t, 0} = H_t - \sum_{s=1}^{\eta} h_{t-s, s}, \sum_{s=-1, 1, \dots, \eta} h_{t, s} = I_t - H_t + \sum_{s=1}^{\eta} h_{t-s, s}, R_t \Lambda_t\right)\right).
\end{aligned}$$

Finally,

$$\mathbb{P}(H_t, I_t | \mathcal{F}_{t-1}) = \sum_{h_{t-\eta, \eta}, \dots, h_{t-1, 1}} \mathbb{P}(H_t, I_t, h_{t-\eta, \eta}, \dots, h_{t-1, 1} | \mathcal{F}_{t-1}).$$

Therefore, the MCEM approach and the proposed estimation method can still be applied, though the objective functions must be updated accordingly.

III An MCEM algorithm to estimate the model parameters when prior knowledge about ω and $\tilde{\omega}$ is available.

In practice, estimates of ω_s and $\tilde{\omega}_s$ might be available from small biomedical or contact tracing studies. Due to the diversity in sample sizes, the demographics of study cohorts, and the estimation methods employed in different studies, these existing estimates can vary widely. In such cases, it's possible to treat these estimates as prior knowledge and use them to estimate the model parameters with Algorithm 2. In this algorithm, we assume that ω_s and $\tilde{\omega}_s$ can be approximated using the probability density function of gamma distributions, such that

$$\begin{aligned}
\omega_s(c) &= \mathbb{P}\left(s-1 \leq \text{Gamma}(k_1(c), \mu_1(c)) \leq s\right), \quad s = 1, \dots, \eta-1, \\
\tilde{\omega}_s(c) &= \mathbb{P}\left(s \leq \text{Gamma}(k_2(c), \mu_2(c)) \leq s+1\right), \quad s = 0, \dots, \tilde{\eta}, \\
\text{and} \quad \omega_{\eta}(c) &= 1 - \sum_{s=1}^{\eta-1} \omega_s(c), \quad \tilde{\omega}_{-1}(c) = 1 - \sum_{s=1}^{\tilde{\eta}} \tilde{\omega}_s(c),
\end{aligned}$$

where $(k_1(c), \mu_1(c), k_2(c), \mu_2(c))$ are the shape and rate parameters of the gamma distribution and $c \in \mathcal{C}$ is the index of prior studies that generated the estimates of ω_s and $\tilde{\omega}_s$. We propose to assign probability weights W_c to each candidate estimate of ω and $\tilde{\omega}$ and assume that the true values of ω_s and $\tilde{\omega}_s$ can be calculated as a weighted average from these studies. A pseudo-code algorithm is shown in Algorithm 2.

Algorithm 2 An MCEM algorithm for estimating the model parameters when prior knowledge of ω_s and $\tilde{\omega}_s$ is available.

Assign probability weights W_c , $c \in \mathcal{C}$, to candidate estimate $(\omega(c), \tilde{\omega}(c))$.

for $c \in \mathcal{C}$, **do**

Require: initial parameter value $\gamma^{(0)}(c) = (\beta^{(0)}(c), \theta^{(0)}(c), \omega(c), \tilde{\omega}(c))$, $k \leftarrow 0$, and the break-point critical value Δ_0 .

while $\|\gamma^{(k+1)}(c) - \gamma^{(k)}(c)\|_\infty > \Delta_0$, **do**

for $0 \leq r \leq t$, $1 \leq m \leq N_0$, **do**

Sample $Data_{miss,r}^{(m,k)}$ from $\mathbb{P}_{\gamma^{(k)}(c)}(H_r, I_r, Data_{miss,r} | \mathcal{F}_{r-1})$ derived in (8)

end for

Calculate the Monte Carlo Q-function $\hat{Q}(\gamma | \gamma^{(k)}(c))$,

Seek for the estimate $\gamma^{(k+1)}(c) = \arg \max_{\gamma \in \Gamma} \hat{Q}(\gamma | \gamma^{(k)}(c))|_{\omega=\omega(c), \tilde{\omega}=\tilde{\omega}(c)}$.

let $k \leftarrow k + 1$.

end while

Take the estimate from the final iteration $\gamma^{(k+1)}(c)$ as $\gamma(c)$.

end for

Output the final estimate, which is given by $\hat{\gamma} = (\sum_{c \in \mathcal{C}} W_c \gamma(c)) / (\sum_{c \in \mathcal{C}} W_c)$.

In our local data generating process, we used an infectiousness function that mimicked the reported serial interval from [Li et al. \(2020\)](#). However, for the data analysis, we applied an infectiousness function derived from a meta-analysis of results from [Wu et al. \(2020\)](#); [Ali et al. \(2020\)](#); [Chen et al. \(2022\)](#); [Deng et al. \(2021\)](#), using it as the initial value for estimating the infectiousness function parameters. We presenting the information here for reference,

For infectiousness function:

1. In [Li et al. \(2020\)](#), the estimated infectiousness function follows a Gamma distribution with a mean of 7.5 days (95% CI, [5.3, 19]). This corresponds to a standard deviation ranging approximately from 1.12 to 5.86. In our simulation, we set the infectiousness profile using a Gamma distribution with shape and scale parameters of 2.5 and 3, respectively, resulting in a mean of 7.5 and a standard deviation of 4.74.
2. In [Wu et al. \(2020\)](#), the estimated infectiousness function has a gamma distribution with mean 7.0 and standard deviation 4.5.
3. In [Ali et al. \(2020\)](#), the estimated serial interval (that we used to approximate the infectiousness function) has a normal distribution with mean 5.1 and standard deviation 5.3.
4. In [Chen et al. \(2022\)](#), the estimated temporal generation time distribution (that we used to approximate the infectiousness function) is given by Weibull distribution with mean 5.20 and standard deviation 3.65.
5. In [Deng et al. \(2021\)](#), the estimated incubation period (that we used to approximate the infectiousness function) is given by a gamma distribution with mean 2.73 and standard deviation 1.23.

Similarly, our hospitalization propensity was set using a Gamma distribution to mimic the distribution of the delay between illness onset and hospitalization reported in [Li et al. \(2020\)](#).

IV Additional clarification on the simulation process and guidance on model selection for real-world applications

The simulated COVID-19 incidence curve and social distancing variable, designed to mimic the Unacast data, are shown below in Figure S2.

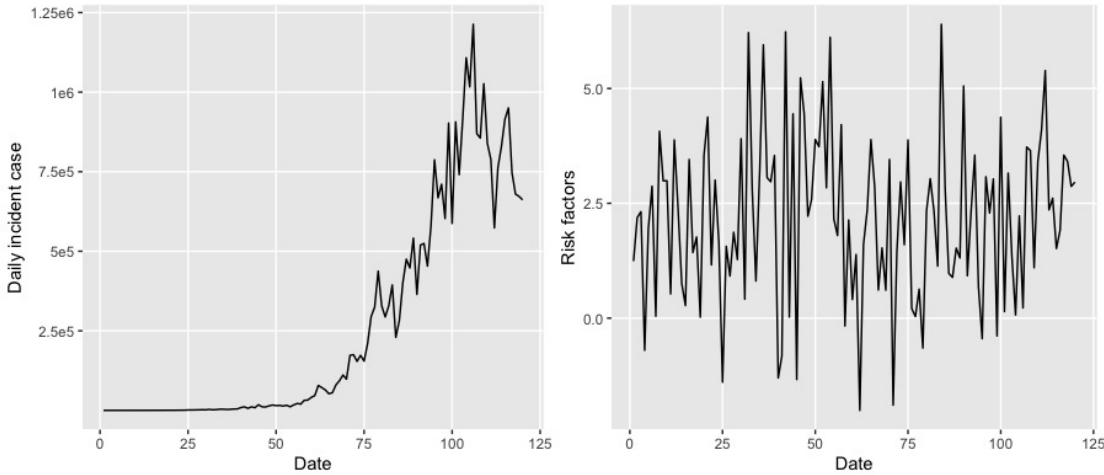


Figure S2: The left panel shows the simulated COVID-19 incidence curves, while the right panel displays simulated risk factor data, representing the percentage change in visits to nonessential businesses (based on Unacast data) after applying a logistic transformation.

In our real data application, the model was selected using the following procedure:

Selection of risk factors: The risk factors in our model were selected based on a thorough review of the literature that has extensively examined local factors influencing COVID-19 transmission. Studies such as [Talic et al. \(2021\)](#) on the effectiveness of social distancing measures, [Weaver et al. \(2022\)](#) on environmental determinants, and [Rubin et al. \(2020\)](#) on the role of population density, among others, have consistently shown that factors like social distancing, population density, and environmental conditions (such as temperature) are significantly associated with disease transmission. Although temperature may have a smaller effect, its influence is still relevant and was therefore included in our analysis.

When using the proposed method, including variables that are genuinely associated with R_t enhances model performance, while including unrelated variables can introduce noise and reduce efficiency, as they do not improve estimation accuracy nor aid in identifying relevant risk factors. While risk factor selection is not the primary theoretical focus of the method, it is an important practical component in real-world applications. To assist users in risk factor selection, we propose the following practical guidelines:

- Conduct a comprehensive literature review and consult with domain experts to identify strong candidate risk factors.
- Ensure the availability of reliable data and assess the correlation between potential risk factors and R_t .
- Avoid multicollinearity and focus on variables that are most relevant to R_t .

Model selection: We focus on the discussion of model diagnostics and model selection for the time series component of the proposed method. In our data application, we applied the Box-Cox transformation to the preliminary R_t estimates obtained using Cori's method to determine an appropriate link function. The estimated lambda values for each county ranged from -1 to 0.5, with an overall estimate between 0 and 0.5, leading us to use the log link function. Subsequently, we fitted a generalized linear mixed-effects model with the R_t estimated by Cori's method as the outcome and the selected risk factors as covariates using a log link function. After applying the log link function, we calculated the residuals and examined the partial autocorrelation function (PACF) of the residuals by county to determine the appropriate order for an autoregressive (AR) model. The PACF plot indicated an AR(1) structure for three of the four counties and an AR(2) structure for one county. For model parsimony, we opted to use an AR(1) structure for the overall model.

In general, one may begin by obtaining preliminary estimates of the reproduction number from observed incidence data using Cori's estimator. A time series model can then be fitted to these estimates along with exogenous variables, following standard time series modeling procedures.

- Data Transformation: Apply the Box-Cox transformation to stabilize variance over time, typically using a logarithmic transformation, as it often improves model fit in time series data.
- Decomposition: Decompose the time series into trend, seasonal, and noise components using STL (seasonal-trend decomposition via LOESS). The trend component can be estimated through non-parametric regression or a simple linear model. This decomposition allows for isolating the underlying structure from random fluctuations.
- Noise Modeling and ARIMA Selection: To model the noise component, use ACF and PACF plots to select the ARIMA model order, then refine the selection using criteria like AIC or BIC to balance fit and complexity.
- High-Dimensional Variable Selection: When working with many exogenous variables, an information-based selection method can help identify a relevant subset, minimizing model complexity while retaining the most significant covariates.

V A comparison of the estimated R_t to reference approach with different sliding window

The Figure 2 uses a 3-day sliding window chosen from the criteria of minimizing the L^2 distance between the estimated and oracle sequences of R_t . We observed that R_t estimated at the window midpoint generally had a smaller bias compared to R_t estimated at the window endpoint, which was consistent with the results of [Gostic et al. \(2020\)](#) and [Gressani et al. \(2023\)](#). However, for the majority of time points (e.g., 45 out of 57 days as shown in Fig.2, 78.9%), our proposed method consistently produced estimates with smaller bias than Cori's method, regardless of whether R_t was reported at the window's endpoint or midpoint. The magnitude of bias reduction is substantial, as shown in Figure 2.

1-day sliding window: When using a 1-day sliding window, Cori's R_t estimates performed similarly to or even slightly better than the proposed estimates in the later stage of the simulated period, where the daily incident cases I_t were large enough ($\geq 5 \times 10^4$) for Cori's method to estimate R_t accurately without incorporating hospitalization data, as shown in Figure S3. For both methods, the bias was of the order $O(10^{-2})$ during this period.

However, Cori's estimates showed a substantial bias in the early stage of the simulated period when the incident cases I_t were small ($\leq 2 \times 10^3$), while our proposed estimates maintained a small bias by incorporating hospitalization data, as shown in Figure S4. During this period, the proposed estimator showed consistent performance with bias of the order $O(10^{-2})$, whereas Cori's estimator had a much larger bias, on the order of $O(10^{-1})$ (or even $O(1)$). This suboptimal performance of Cori's method in the early stage is also why the data-driven window length selection resulted in a 3-day sliding window instead of a 1-day window.

In general, the 1-day sliding window limits Cori's method's ability to borrow information from nearby days, leading to unsatisfactory performance when daily incident cases I_t are small. This drawback becomes even more pronounced when estimating R_t in smaller populations, such as a county with roughly 10 cases per day. In contrast, our proposed method is less affected in these cases as it leverages both incidence and hospitalization data.

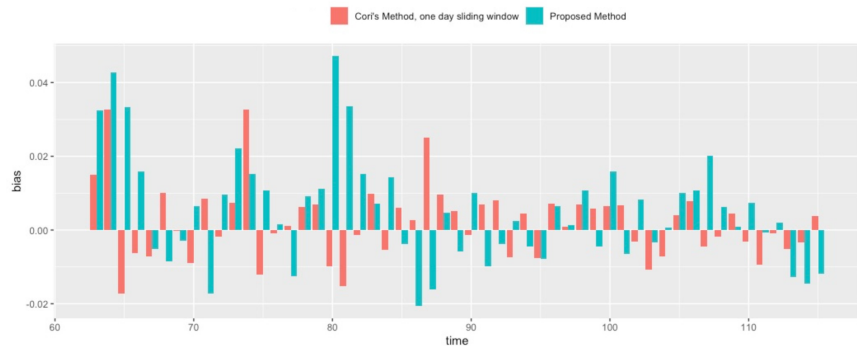


Figure S3: Comparison of the estimation bias of R_t between the proposed method and Cori's method using a 1-day sliding window for Cori's method, during the later stage of the simulated period when I_t is large.

7-day sliding window: When using a 7-day sliding window, reporting R_t at the midpoint for Cori's method resulted in smaller bias compared to reporting at the endpoint. However, the overall bias was much larger compared to using Cori's method with a 3-day sliding window or our proposed method, as the 7-day window tended to oversmooth the estimates. Given the significantly larger bias relative to our proposed method, we illustrate the comparison using a randomly selected simulated dataset, rather than a bar plot of the bias, as shown in Figure S5.

VI A simulation scenario with under-reported incidence and hospitalization data

In this scenario, we generate the data where both incidence and hospitalization data were subject to under-reporting, with daily reporting rates fluctuating randomly between 0% and 30%. Under this condition, the estimation bias of R_t increased in our proposed method, but remained significantly smaller than the bias observed in Cori's method, as shown in Figure S6. This indi-

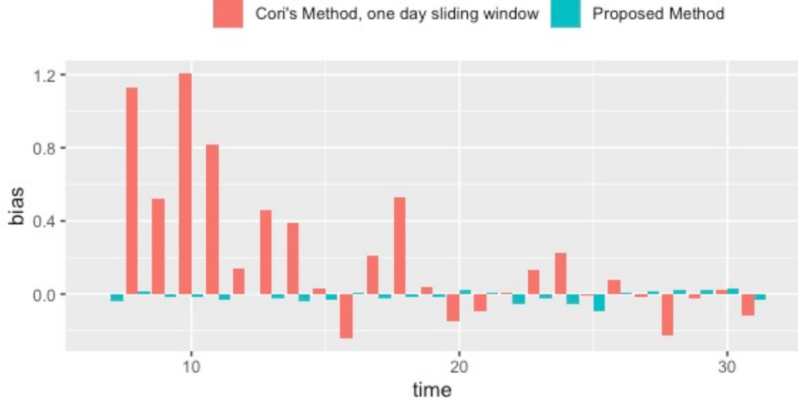


Figure S4: Comparison of the estimation bias of R_t between the proposed method and Cori's method using a 1-day sliding window for Cori's method, during the early stage of the simulated period when I_t is small.

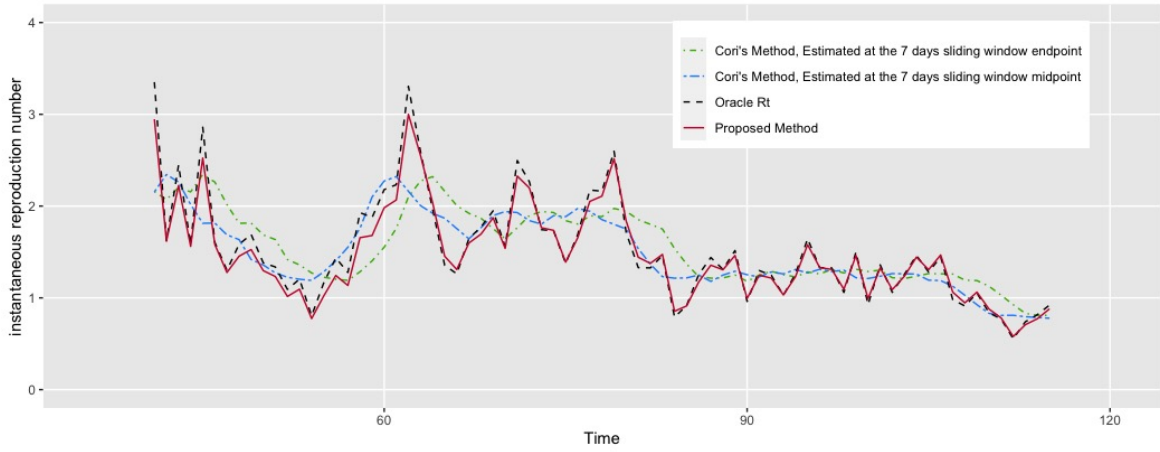


Figure S5: Comparison of the estimation bias of R_t between the proposed method and Cori's method using a 7-day sliding window for Cori's method.

cates that the proposed method retains a degree of robustness to data inaccuracies, even when the hospitalization data are imperfect.

VII Detailed proof of technique results

Proof. of Lemma 1. According to (1) and (3), notice that, conditional on $\mathcal{F}_{t-1} \triangleq \sigma\{I_s, s \leq t-1\}$,

$$\begin{aligned}
 \mathbb{P}(h_{t,u_1}, h_{t,u_2} | \mathcal{F}_{t-1}) &= \sum_{I_t} \mathbb{P}(h_{t,u_1}, h_{t,u_2} | I_t) \cdot \mathbb{P}(I_t | I_0, \dots, I_{t-1}) \\
 &= \sum_{I_t=h_{t,u_1}+h_{t,u_2}}^{\infty} \left[\frac{I_t!}{h_{t,u_1}! h_{t,u_2}!} \tilde{\omega}_{u_1}^{h_{t,u_1}} \tilde{\omega}_{u_2}^{h_{t,u_2}} \cdot \frac{(1 - \tilde{\omega}_{u_1} - \tilde{\omega}_{u_2})^{I_t - h_{t,u_1} - h_{t,u_2}}}{(I_t - h_{t,u_1} - h_{t,u_2})!} \right. \\
 &\quad \left. \cdot \frac{(R_t \Lambda_t)^{I_t}}{I_t!} e^{-R_t \Lambda_t} \right] \\
 &= \frac{(\tilde{\omega}_{u_1} R_t \Lambda_t)^{h_{t,u_1}}}{h_{t,u_1}!} e^{-\tilde{\omega}_{u_1} R_t \Lambda_t} \cdot \frac{(\tilde{\omega}_{u_2} R_t \Lambda_t)^{h_{t,u_2}}}{h_{t,u_2}!} e^{-\tilde{\omega}_{u_2} R_t \Lambda_t}
 \end{aligned} \tag{14}$$

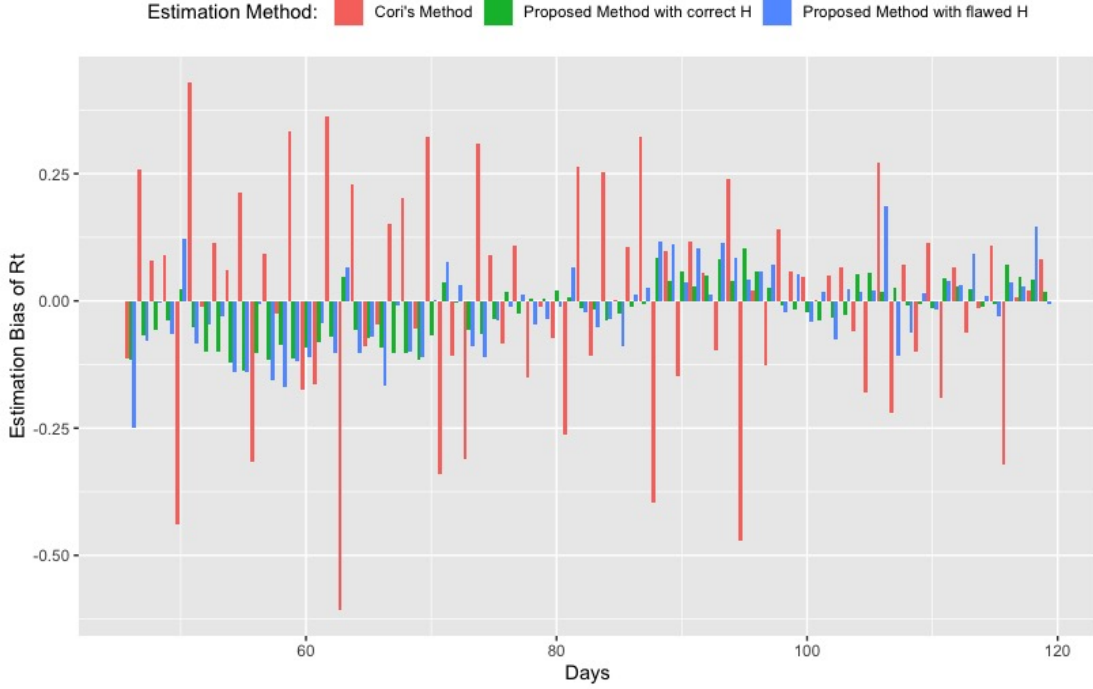


Figure S6: Comparison of estimation bias in R_t using under-reported incidence and hospitalization data.

$$\begin{aligned}
& \cdot \sum_{I_t=h_{t,u_1}+h_{t,u_2}}^{\infty} \frac{((1-\tilde{\omega}_{u_1}-\tilde{\omega}_{u_2})R_t\Lambda_t)^{I_t-h_{t,u_1}-h_{t,u_2}}}{(I_t-h_{t,u_1}-h_{t,u_2})!} e^{-(1-\tilde{\omega}_{u_1}-\tilde{\omega}_{u_2})R_t\Lambda_t} \\
& = \frac{(\tilde{\omega}_{u_1}R_t\Lambda_t)^{h_{t,u_1}}}{h_{t,u_1}!} e^{-\tilde{\omega}_{u_1}R_t\Lambda_t} \cdot \frac{(\tilde{\omega}_{u_2}R_t\Lambda_t)^{h_{t,u_2}}}{h_{t,u_2}!} e^{-\tilde{\omega}_{u_2}R_t\Lambda_t}.
\end{aligned}$$

Hence (7) holds and $h_{t,u_1}|\mathcal{F}_{t-1} \perp h_{t,u_2}|\mathcal{F}_{t-1}$. Besides, it's clear that $(h_{t,u_1}, h_{t,u_2})|\mathcal{G}_{t-1} = (h_{t,u_1}, h_{t,u_2})|\mathcal{F}_{t-1}$ from Figure 1, thus proves Lemma 1. \square

Proof. of Theorem 1. Notice that

$$\log \mathbb{P}_\gamma(H_r, I_r | \mathcal{F}_{r-1}) = \log \mathbb{P}_\gamma(H_r, I_r, Data_{miss,r} | \mathcal{F}_{r-1}) - \log \mathbb{P}_\gamma(Data_{miss,r} | \mathcal{D}_{obs,r})$$

therefore,

$$\begin{aligned}
\log \mathbb{P}_\gamma(H_r, I_r | \mathcal{F}_{r-1}) &= \int \log \mathbb{P}_\gamma(H_r, I_r | \mathcal{F}_{r-1}) d\mathbb{P}_{\gamma^{(k)}}(Data_{miss,r} | \mathcal{D}_{obs,r}) \\
&= \int \log \mathbb{P}_\gamma(H_r, I_r, Data_{miss,r} | \mathcal{F}_{r-1}) d\mathbb{P}_{\gamma^{(k)}}(Data_{miss,r} | \mathcal{D}_{obs,r}) \\
&\quad - \int \log \mathbb{P}_\gamma(Data_{miss,r} | \mathcal{D}_{obs,r}) d\mathbb{P}_{\gamma^{(k)}}(Data_{miss,r} | \mathcal{D}_{obs,r}) \\
&\triangleq \mathbb{E}_{\gamma^{(k)}} \left(\log \mathbb{P}_\gamma(H_r, I_r, Data_{miss,r} | \mathcal{F}_{r-1}) | \mathcal{D}_{obs,r} \right) - H_r(\gamma | \gamma^{(k)})
\end{aligned}$$

Since $H_r(\gamma|\gamma^{(k)}) \leq H_r(\gamma^{(k)}|\gamma^{(k)})$ for arbitrary $\gamma \in \Gamma$ and $0 \leq r \leq t$ according to the information inequality (Gibbs inequality), hence

$$\begin{aligned}\ell_C(\gamma^{(k+1)}) - \ell_C(\gamma^{(k)}) &= \sum_{0 \leq r \leq t} \log \mathbb{P}_{\gamma^{(k+1)}}(H_r, I_r | \mathcal{F}_{r-1}) - \sum_{0 \leq r \leq t} \log \mathbb{P}_{\gamma^{(k)}}(H_r, I_r | \mathcal{F}_{r-1}) \\ &= Q(\gamma^{(k+1)}|\gamma^{(k)}) - Q(\gamma^{(k)}|\gamma^{(k)}) + \sum_{0 \leq r \leq t} (H_r(\gamma^{(k)}|\gamma^{(k)}) - H_r(\gamma^{(k+1)}|\gamma^{(k)})) \\ &\geq Q(\gamma^{(k+1)}|\gamma^{(k)}) - Q(\gamma^{(k)}|\gamma^{(k)}) \geq 0,\end{aligned}$$

which finishes the proof. \square

Proof. of Theorem 2. First, since the composite log-likelihood ℓ_C is smooth in γ in a finite Euclidean space and the parameter space Γ inherited the norm from the same Euclidean space, so ℓ_C is continuous in Γ and is differentiable in the interior of Γ . Besides, since Γ is compact, so for an arbitrary sample point, and an arbitrary parameter point $\dot{\gamma}$ with $\ell_C(\dot{\gamma}) > -\infty$, the set

$$\Gamma(\dot{\gamma}) \triangleq \{\gamma \in \Gamma : \ell_C(\gamma) \geq \ell_C(\dot{\gamma})\}$$

is bounded. For any convergence sequence $\{\ddot{\gamma}_n \in \Gamma(\dot{\gamma})\}_{n \geq 1}$, with $\ddot{\gamma}_n \rightarrow \ddot{\gamma}$, we have $\ddot{\gamma} \in \Gamma$ since Γ is compact and each $\ddot{\gamma}_n \in \Gamma(\dot{\gamma}) \subset \Gamma$; also, $\ell_C(\ddot{\gamma}_n) \geq \ell_C(\dot{\gamma})$ for each n implies $\ell_C(\ddot{\gamma}) \geq \ell_C(\dot{\gamma})$. Therefore, $\ddot{\gamma} \in \Gamma(\dot{\gamma})$ and according to Heine-Borel theorem, we conclude that $\Gamma(\dot{\gamma})$ is also a compact set for an arbitrary sample point and parameter point $\dot{\gamma}$. Second, with an arbitrary but fixed sample point, define Γ_s as the set of stationary point generated by function $M(\cdot) \triangleq \arg \max_{\gamma \in \Gamma} Q(\gamma|\cdot)$, i.e.,

$$\Gamma_s = \left\{ \gamma_s \in \Gamma : \gamma_s = M(\gamma_s) \right\} = \left\{ \gamma_s \in \Gamma : Q(\gamma_s|\gamma_s) = \max_{\gamma \in \Gamma} Q(\gamma|\gamma_s) \right\}$$

Since function $Q(x|y)$ is smooth in both x and y , so for an arbitrary convergence sequence $\{\gamma_{s,n} \in \Gamma_s\}_{n \geq 1}$ with $\gamma_{s,n} \rightarrow \gamma_{s,0}$, and arbitrary γ , we have

$$Q(\gamma|\gamma_{s,0}) = \lim Q(\gamma|\gamma_{s,n}) \leq \lim Q(\gamma_{s,n}|\gamma_{s,n}) = Q(\gamma_{s,0}|\gamma_{s,0}). \quad (15)$$

Because γ is arbitrary in (15), so $\gamma_{s,0} \in \Gamma_s$ and hence Γ_s is compact. Further we conclude that, $M(\cdot)$ is closed over the complement of Γ_s since $M(\cdot)$ is identical mapping over the compact set Γ_s . Third, with the arbitrary but fixed sample point, ℓ_C is a continuous map on Γ , and for an arbitrary point $\gamma \in \Gamma_s$, we have $\ell_C(M(\gamma)) = \ell_C(\gamma)$, while for an arbitrary point $\gamma \notin \Gamma_s$, we have $Q(M(\gamma)|\gamma) > Q(\gamma|\gamma)$, hence

$$\ell_C(M(\gamma)) - \ell_C(\gamma) \geq Q(M(\gamma)|\gamma) - Q(\gamma|\gamma) > 0.$$

Combine the above three conclusions, the global convergence theorem in [Wu \(1983\)](#) and [Willard \(1969\)](#) implies that for an arbitrary sample point, our EM-algorithm estimates $\gamma^{(k)}$ converges to a stationary point γ_s in the stationary set Γ_s induced by the function $M(\cdot) \triangleq \arg \max_{\gamma \in \Gamma} Q(\gamma|\cdot)$ when $k \rightarrow \infty$, and $\ell_C(\gamma^{(k)})$ converge monotonically to $\ell_C(\gamma_s)$. \square

Proof. of Theorem 3. To avoid confusion, we denote $E_\gamma(\cdot)$ as the expectation evaluated under the $P_\gamma(\cdot)$, the probability measure induced by $\{H_t, I_t\}$ who follows the distribution in the proposed model with parameter $\gamma = (\beta, \theta)$. To distinguish the oracle parameter value, we denote it as γ_0 .

Now, for fixed infectiousness function $\{\omega_s, s = 1, \dots, \eta\}$ and hospitalization propensity $\{\tilde{\omega}_s, s = -1, \dots, \tilde{\eta}\}$, we have

$$\begin{aligned}
\ell_C &= \sum_{0 \leq r \leq t} \log \mathbb{P}(H_r, I_r | \mathcal{F}_{r-1}) \\
&= \sum_{0 \leq r \leq t} \log \sum_{h_{r-\tilde{\eta}}, \dots, h_{r-1,1}} \mathbb{P}(H_r, I_r, h_{r-\tilde{\eta}}, \dots, h_{r-1,1} | \mathcal{F}_{r-1}) \\
&= \sum_{0 \leq r \leq t} \log \sum_{h_{r-\tilde{\eta}}, \dots, h_{r-1,1}} \mathbb{P}\left(Poisson(\tilde{\omega}_0 R_r \Lambda_r) = H_r - \sum_{s=1}^{\tilde{\eta}} h_{r-s,s}\right) \\
&\quad \cdot \prod_{s=1}^{\tilde{\eta}} \mathbb{P}\left(Binomial(I_{r-s}, \tilde{\omega}_s) = h_{r-s,s}\right) \mathbb{1}\left(H_r - I_r \leq \sum_{s=1}^{\tilde{\eta}} h_{r-s,s} \leq H_r\right) \\
&\quad \cdot \mathbb{P}\left(Poisson((1 - \tilde{\omega}_0) R_r \Lambda_r) = I_r - H_r + \sum_{s=1}^{\tilde{\eta}} h_{r-s,s}\right), \\
&= \sum_{0 \leq r \leq t} \log \left[(R_r)^{I_r} \exp(-R_r \Lambda_r) C_r \right] \\
&= \sum_{0 \leq r \leq t} \left[I_r \log(R_r) - R_r \Lambda_r + \log C_r \right]
\end{aligned}$$

where

$$C_r = \Lambda_r^{I_r} (1 - \tilde{\omega}_0)^{I_r} \sum_{h_{r-\tilde{\eta}}, \dots, h_{r-1,1}} \frac{\left(\frac{\tilde{\omega}_0}{1-\tilde{\omega}_0}\right)^{H_r - \sum_{s=1}^{\tilde{\eta}} h_{r-s,s}} \prod_{s=1}^{\tilde{\eta}} \mathbb{P}(h_{r-s,s} | \mathcal{F}_{r-1})}{(H_r - \sum_{s=1}^{\tilde{\eta}} h_{r-s,s})! (I_r - H_r + \sum_{s=1}^{\tilde{\eta}} h_{r-s,s})!}$$

are constants as functions of γ .

Thus,

$$\hat{\gamma} = \arg \max_{\gamma \in \Gamma} \sum_{0 \leq r \leq t} \left[I_r \log(R_r) - R_r \Lambda_r \right].$$

Meanwhile, under Condition 1, we have

$$\frac{t_0}{t} \sum_{s=1}^t \{I_s \log(R_s) - R_s \Lambda_s\} \xrightarrow{a.s.} E_{\gamma_0} \sum_{0 \leq r \leq t_0} \left[I_r \log(R_r) - R_r \Lambda_r \right] \quad (16)$$

for some $t_0 > 0$. We now demonstrate that the maximum of the right-hand-side of (16) over $\gamma \in \Gamma$ is attained uniquely at $\gamma = \gamma_0$. Let $\ell_{Q,r}(\gamma) = (R_r)^{I_r} \exp[-R_r \Lambda_r]$. By Jensen's Inequality, for arbitrary $\gamma_1 \in \Gamma$, we have

$$\sum_{0 \leq r \leq t_0} E_{\gamma_0} \left(\log \frac{\ell_{Q,r}(\gamma_1)}{\ell_{Q,r}(\gamma_0)} \right) \leq \sum_{0 \leq r \leq t_0} \log E_{\gamma_0} \left(\frac{\ell_{Q,r}(\gamma_1)}{\ell_{Q,r}(\gamma_0)} \right) = 0,$$

Hence

$$\sum_{0 \leq r \leq t_0} E_{\gamma_0} \left[\log \ell_{Q,r}(\gamma_1) \right] \leq \sum_{0 \leq r \leq t_0} E_{\gamma_0} \left[\log \ell_{Q,r}(\gamma_0) \right]$$

for arbitrary $\gamma_1 \in \Gamma$, and the equality holds if and only if $\ell_{Q,r}(\gamma_1) = \ell_{Q,r}(\gamma_0)$ almost surely. We denote B^c to be the zero-measure set of the parameter space Γ such that Condition 1 holds for all $\omega \in B$. If, on the contrary that $\hat{\gamma} \not\rightarrow \gamma_0$, then there exist a positive constant $\delta > 0$ and a subsequence $\{t_{k1}, t_{k2}, \dots, t_{kn}, \dots\}$ such that $|\hat{\gamma}(t_{ki}) - \gamma_0| \geq \delta$ for $i = 1, 2, \dots, n, \dots$. By the compactness of Γ , there further exists a sub-subsequence $\{t_{u_{m1}}, t_{u_{m2}}, \dots, t_{u_{mn}}, \dots\}$ such that $\{\hat{\gamma}_{t_{u_{mi}}}\}_{i \geq 1}$ is a convergence sub-subsequence and $\hat{\gamma}(t_{u_{mn}}) \rightarrow \gamma^*$ for some $\gamma^* \neq \gamma_0$. Then,

$$\begin{aligned} \lim_{n \rightarrow \infty} \frac{t_0}{t_{u_{mn}}} \sum_{s=1}^{t_{u_{mn}}} \log \ell_{Q,r}(\hat{\gamma}(t_{u_{mn}})) &\geq \lim_{n \rightarrow \infty} \frac{t_0}{t_{u_{mn}}} \sum_{s=1}^{t_{u_{mn}}} \log \ell_{Q,r}(\gamma_0) = E_{\gamma_0} \sum_{s=1}^{t_0} \log \ell_{Q,r}(\gamma_0) \\ &> E_{\gamma_0} \sum_{s=1}^{t_0} \log \ell_{Q,r}(\gamma^*) = \lim_{n \rightarrow \infty} \frac{t_0}{t_{u_{mn}}} \sum_{s=1}^{t_{u_{mn}}} \log \ell_{Q,r}(\gamma^*) \\ &= \lim_{n \rightarrow \infty} \frac{t_0}{t_{u_{mn}}} \sum_{s=1}^{t_{u_{mn}}} \log \ell_{Q,r}(\hat{\gamma}(t_{u_{mn}})), \end{aligned}$$

which is a contradiction. Hence, $\hat{\gamma} \rightarrow \gamma_0$ for each $\omega \in B$, i.e., the strong consistency holds for $\hat{\gamma}$. \square

Proof. of Theorem 4. Define

$$U_t(\gamma) = \sum_{0 \leq r \leq t} \frac{\partial \log \ell_{Q,r}(\gamma)}{\partial \gamma} = \sum_{0 \leq r \leq t} \left(\frac{\partial R_r}{\partial \gamma} \right)^T R_r^{-1} (I_r - R_r \Lambda_r) \triangleq \sum_{0 \leq r \leq t} \xi_r(\gamma),$$

and let

$$A_t^2 = \sum_{0 \leq r \leq t} \text{Cov}(\xi_r(\gamma_0) \mid \mathcal{F}_{r-1})$$

Then the proofs are identical to those of theorem 4.1 in [Shi et al. \(2022\)](#), so we only provide an outline of the proof here.

Since $\hat{\gamma}$ satisfy $U_t(\hat{\gamma}) = 0$, so by Taylor expansion, we have

$$0 = U_t(\hat{\gamma}) = U_t(\gamma_0) + \frac{\partial U_t(\gamma)}{\partial \gamma} \Big|_{\gamma=\hat{\gamma}} (\hat{\gamma} - \gamma_0), \quad i.e., \quad (1)$$

$$- A_t^{-1} \frac{\partial U_t(\gamma)}{\partial \gamma} \Big|_{\gamma=\hat{\gamma}} (A_t^{-1})^T A_t (\hat{\gamma} - \gamma_0) = A_t^{-1} U_t(\gamma_0). \quad (17)$$

For an arbitrary given and fixed vector $\alpha = (\alpha_1, \dots, \alpha_{p+2})^T \in \mathcal{M}_{(p+2) \times 1}$, define

$$S_t(\alpha) \triangleq \frac{\alpha^T}{\|\alpha\|} A_t^{-1} U_t(\gamma_0) = \sum_{0 \leq r \leq t} \frac{\alpha^T}{\|\alpha\|} A_t^{-1} \left(\left(\frac{\partial R_r}{\partial \gamma} \right)^T R_r^{-1} (I_r - R_r \Lambda_r) \right) \triangleq \sum_{0 \leq r \leq t} \tilde{\xi}_r.$$

It's trivial to see that $\tilde{\xi}_r \in \mathcal{F}_r$ and $\mathbb{E}(\tilde{\xi}_r | \mathcal{F}_{r-1}) = 0$, hence $\{\tilde{\xi}_r, 0 \leq r \leq t\}$ is a martingale difference sequence. So

$$\tilde{V}_t^2(\alpha) \triangleq \sum_{0 \leq r \leq t} \mathbb{E}(\tilde{\xi}_r^2 | \mathcal{F}_{r-1}) = \frac{\alpha^T}{\|\alpha\|} A_t^{-1} V_t^2(\gamma_0) (A_t^{-1})^T \frac{\alpha}{\|\alpha\|}$$

with $V_t^2(\gamma) \triangleq \sum_{0 \leq r \leq t} \mathbb{E}(\xi_r^2(\gamma) | \mathcal{F}_{r-1})$, is the conditional variance that would affect the limiting distribution of $S_t(\alpha)$. Under Condition 2, we have

$$\tilde{V}_t^2(\alpha) \xrightarrow{P} \zeta^2(\alpha)$$

Together with Condition 3, we conclude that $\tilde{V}_t^2(\alpha) \xrightarrow{L_1} \zeta^2(\alpha)$ and $\mathbb{E}\tilde{V}_t^2(\alpha) = \mathbb{E}\zeta^2(\alpha) = 1$. Hence $\mathbb{E}(\max_{0 \leq r \leq t} \tilde{\xi}_r^2) \leq 1$. Combining the conditional Lindeberg condition (Condition 4), we conclude $\tilde{U}_t^2(\alpha) - \tilde{V}_t^2(\alpha) \xrightarrow{L_1} 0$ by theorem 2.23 of [Hall and Heyde \(2014\)](#) for $\tilde{U}_N^2(\alpha) \triangleq \sum_{0 \leq r \leq t} \tilde{\xi}_r^2$, hence $\tilde{U}_t^2(\alpha) \xrightarrow{L_1} \zeta^2(\alpha)$.

Thus, by using the martingale central limit theorem (see e.g, theorem 3.2 of [Hall and Heyde \(2014\)](#)), $A_t^{-1} U_t(\gamma_0)$ converge to certain distribution with characteristic function

$$f_{A_t^{-1} U_t(\gamma)}(\alpha) = \mathbb{E} \exp \left(i \alpha^T A_t^{-1} U_t(\gamma_0) \right) \rightarrow \mathbb{E} \exp \left(-\frac{1}{2} \|\alpha\|_2^2 \zeta^2(\alpha) \right),$$

for arbitrary α , or equivalently,

$$A_t^{-1} U_t(\gamma_0) \xrightarrow{d} \zeta^T \cdot Z \quad (\text{stably}),$$

for ζ independent of $Z \sim \mathcal{N}(0, I)$. Of course, the limit distribution holds only on the non-extinction set $\mathcal{E}_{\text{none}}$. Since ζ, Z are also measurable, so we have

$$A_t^{-1} U_t(\gamma_0) \xrightarrow{P} \zeta^T \cdot Z. \quad (18)$$

Now, combining Condition 5 and Theorem 3 insures $\hat{\gamma} \rightarrow_{a.s.} \gamma_0$, i.e., $\hat{\gamma}$ would be in the neighborhood of γ_0 , so we have

$$A_t^{-1} \left(-\frac{\partial U_t(\gamma)}{\partial \gamma} \Big|_{\gamma=\hat{\gamma}} \right) (A_t^{-1})^T \xrightarrow{P} \zeta^T \zeta. \quad (19)$$

Thus, by (17), (18), (19), and our choice of A_t^2 , we conclude that,

$$\left[\sum_{1 \leq r \leq t} \text{Cov}(\xi_r(\gamma_0) | \mathcal{F}_{r-1}) \right]^{1/2} (\hat{\gamma} - \gamma_0) \xrightarrow{d} N(0, I),$$

which finishes the proof. \square

VIII Additional results from the simulation study and application to COVID-19 Data

References

Ali, S. T., Wang, L., Lau, E. H., Xu, X.-K., Du, Z., Wu, Y., Leung, G. M. and Cowling, B. J. (2020), 'Serial interval of SARS-CoV-2 was shortened over time by nonpharmaceutical interventions', *Science* **369**(6507), 1106–1109.

Chen, D., Lau, Y.-C., Xu, X.-K., Wang, L., Du, Z., Tsang, T. K., Wu, P., Lau, E. H., Wallinga, J., Cowling, B. J. et al. (2022), ‘Inferring time-varying generation time, serial interval, and incubation period distributions for COVID-19’, *Nature Communications* **13**(1), 7727.

Cori, A., Ferguson, N. M., Fraser, C. and Cauchemez, S. (2013), ‘A new framework and software to estimate time-varying reproduction numbers during epidemics’, *American Journal of Epidemiology* **178**(9), 1505–1512.

Deng, Y., You, C., Liu, Y., Qin, J. and Zhou, X.-H. (2021), ‘Estimation of incubation period and generation time based on observed length-biased epidemic cohort with censoring for covid-19 outbreak in china’, *Biometrics* **77**(3), 929–941.

Gostic, K. M., McGough, L., Baskerville, E. B., Abbott, S., Joshi, K., Tedijanto, C., Kahn, R., Niehus, R., Hay, J. A., De Salazar, P. M. et al. (2020), ‘Practical considerations for measuring the effective reproductive number, R_t ’, *PLoS Computational Biology* **16**(12), e1008409.

Gressani, O., Faes, C. and Hens, N. (2023), ‘An approximate bayesian approach for estimation of the instantaneous reproduction number under misreported epidemic data’, *Biometrical Journal* **65**(6), 2200024.

Hall, P. and Heyde, C. C. (2014), *Martingale limit theory and its application*, Academic press.

Li, Q., Guan, X., Wu, P., Wang, X., Zhou, L., Tong, Y., Ren, R., Leung, K. S., Lau, E. H., Wong, J. Y. et al. (2020), ‘Early transmission dynamics in Wuhan, China, of novel coronavirus–infected pneumonia’, *New England Journal of Medicine* .

Rubin, D., Huang, J., Fisher, B. T., Gasparrini, A., Tam, V., Song, L., Wang, X., Kaufman, J., Fitzpatrick, K., Jain, A. et al. (2020), ‘Association of social distancing, population density, and temperature with the instantaneous reproduction number of SARS-CoV-2 in counties across the United States’, *JAMA Network Open* **3**(7), e2016099–e2016099.

Shi, J., Morris, J. S., Rubin, D. M. and Huang, J. (2022), ‘Robust modeling and inference of disease transmission using error-prone data with application to sars-cov-2’, *arXiv preprint arXiv:2212.08282* .

Talic, S., Shah, S., Wild, H., Gasevic, D., Maharaj, A., Ademi, Z., Li, X., Xu, W., Mesa-Eguiagaray, I., Rostron, J. et al. (2021), ‘Effectiveness of public health measures in reducing the incidence of COVID-19, SARS-CoV-2 transmission, and COVID-19 mortality: systematic review and meta-analysis’, *BMJ* **375**.

Weaver, A. K., Head, J. R., Gould, C. F., Carlton, E. J. and Remais, J. V. (2022), ‘Environmental factors influencing COVID-19 incidence and severity’, *Annual Review of Public Health* **43**(1), 271–291.

Willard, I. (1969), ‘Zangwill nonlinear programming: a unified approach’.

Wu, C. J. (1983), ‘On the convergence properties of the em algorithm’, *The Annals of statistics* pp. 95–103.

Wu, J. T., Leung, K., Bushman, M., Kishore, N., Niehus, R., de Salazar, P. M., Cowling, B. J., Lipsitch, M. and Leung, G. M. (2020), ‘Estimating clinical severity of COVID-19 from the transmission dynamics in Wuhan, China’, *Nature Medicine* **26**(4), 506–510.

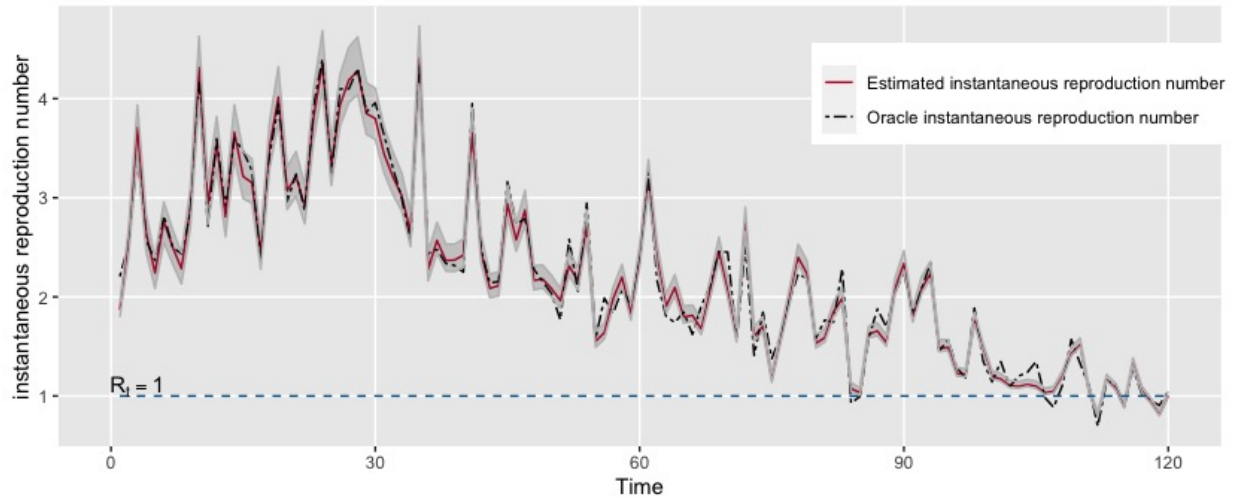


Figure S7: Estimation of the daily instantaneous reproduction number, R_t , when the reported number of daily new infections was accurate, the infectiousness function ω_s and hospitalization propensity $\tilde{\omega}_s$ were unknown and no prior knowledge was available in the simulation study. Black dotted line stands for the oracle R_t . Red solid line and the grey shadow stand for the estimates and its corresponding Bootstrapping confidence interval (90% confidence level) using the proposed method.

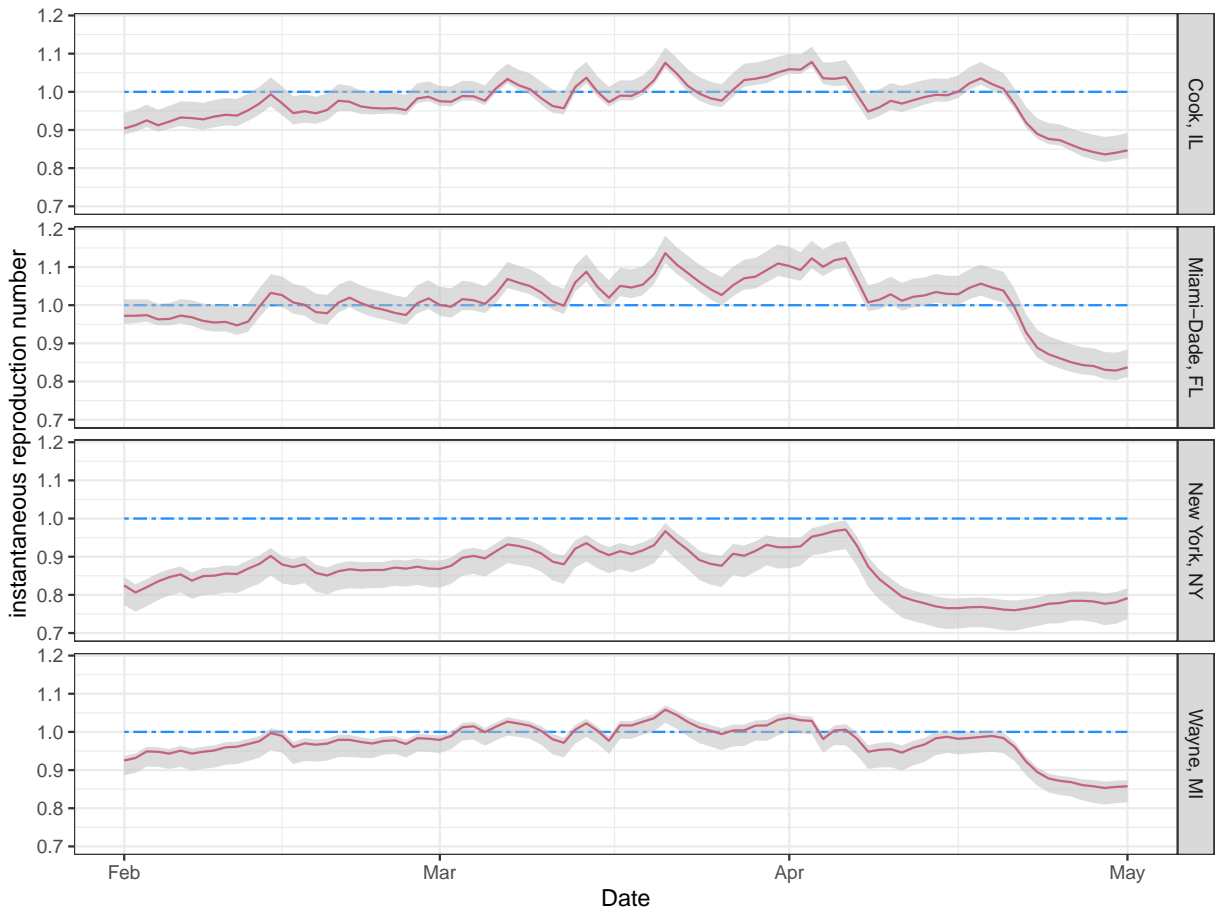


Figure S8: Estimated instantaneous reproduction number, R_t , for COVID-19 in the four studied counties during February to May 2021. The blue lines represent the critical value of $R_t = 1$. Red lines represent the estimated county-level R_t during the study period. Shaded areas indicate the bootstrap confidence intervals (90% confidence level).

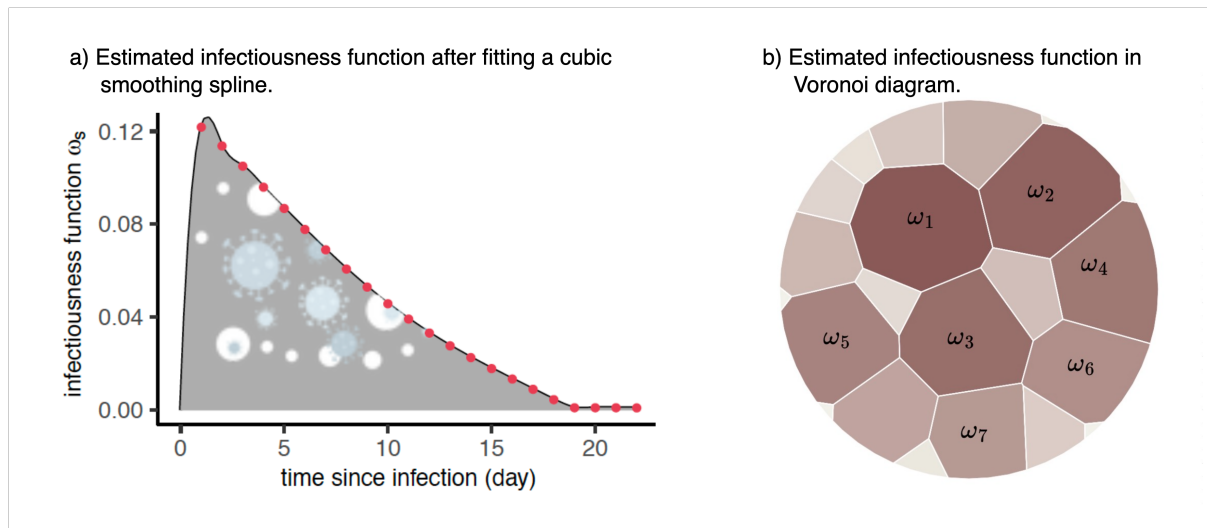


Figure S9: Visualization of the estimated infectiousness function, ω_s , for COVID-19 in the four studied counties during February to May 2021. In panel a), the red dots represent the estimated ω_s , $1 \leq s \leq 22$, while the black line represents the estimated infectiousness function after fitting a cubic smoothing spline. In panel b), the estimated ω_s values are visualized using a Voronoi diagram to compare the magnitude of each ω_s . Values of ω_s in the first week since infection are labeled.